Electronic Structure, Magnetic Properties, ESR, and Optical Spectra for 2-Fe Ferredoxin Models by LCAO-Xα Valence Bond Theory

Louis Noodleman* and Evert Jan Baerends

Contribution from the Department of Theoretical Chemistry, Free University, De Boelelaan 1083, 1081 HV Amsterdam, The Netherlands, and the Department of Chemistry, University of Washington, Seattle, Washington 98195. *Received March 3, 1983*

Abstract: LCAO-Xα valence bond calculations were made to determine the electronic structure of $Fe_2S_2(SH)_4^{2-,3-}$, active site analogues for 2-Fe ferredoxin proteins. Heisenberg coupling constants were calculated for the oxidized and reduced complexes, J(ox.) = -310 cm^{-1} and J(red.) = -73 cm^{-1}. The issue of trapped valence in reduced ferredoxin is analyzed, and it is shown that the Heisenberg Hamiltonian does not properly describe the higher spin states of the reduced form. Various other properties of the ground and electronic excited states are calculated and compared with experimental results on proteins and synthetic analogues. These include the charge-transfer spectrum of the oxidized complex, the Fe d $\rightarrow$ d spectrum of the reduced complex, and the reduced g and A tensors. Charge density difference maps (molecule minus atoms) are constructed for both $2^-/3^-$ forms; comparable experimental X-ray data are not yet available. The nature of the Fe 3d orbital filled by reduction is analyzed; its shape is dependent on the orientation of the SR groups. An indirect mechanism for $2^-/3^-$ reduction is proposed involving cysteine sulfur; at least in some cases, the electron-transfer mechanism should be closely related to the charge-transfer spectrum.

The Fe-S proteins serve as electron transport or catalytic agents in a variety of biological systems.[1-3] They are important components of photosynthetic and respiratory pathways[2] and play a role as well in nitrogen fixation and dehydrogenation reactions.[3] When the variety and importance of the ferredoxins was recognized, a wide array of physical measurements including ESR, ENDOR, magnetic susceptibility, Mössbauer studies, optical spectra, redox potential, and X-ray structure was made on proteins and synthetic analogues.[4-12] The Fe-S proteins include those having 1, 2, 3, and 4 Fe sites.[1,10,13] We will focus here on the 2-Fe ferredoxins having the general formula $Fe_2S_2(SR)_4^{2-,3-}$ where R = cysteine in the proteins and various organic groups in the synthetic analogues.[10-12] Each Fe is roughly tetrahedrally coordinated to the two bridging S atoms (designated S*) and to two of the four SR groups.

That the 2 Fe atoms are high-spin ferric Fe^{3+} (d^5, $S = 5/2$) in the oxidized protein and high-spin Fe^{3+} (d^5, $S_1 = 5/2$) - Fe^{2+} (d^6, $S_2 = 2$) in the reduced is far from obvious. It was first proposed by Gibson et al.[4] that reduced plant ferredoxin contained high-spin Fe^{3+} and Fe^{2+} antiferromagnetically coupled to give a net spin vector $S = 1/2$. This idea was based on the weak ligand field splitting expected for Fe tetrahedrally coordinated to S, favoring high-spin Fe, and on the success of the resulting vector coupling model in rationalizing the observed ESR g values. The semiempirical vector coupling model (based on empirically derived ligand field parameters) has been refined further by Bertrand and Gayda,[14] who showed that the g and A tensor data for a wide variety of plant, animal, and bacterial 2-Fe ferredoxins could be correlated with the model. The vector coupling model of Gibson,[4,10] and the modified model of Bertrand and Gayda[14] are relevant to the Xα valence bond (Xα-VB) calculations we will present.

First principle calculations on Fe-S protein models have been of two types: open-shell Hartree-Fock plus CI (rubredoxin model $Fe(SH)_4^{1-,2-}$) and Xα density functional (rubredoxin, 2-Fe and 4-Fe ferredoxins).[15-20] Open-shell HF-CI calculations on $Fe(SH)_4^{1-,2-}$ and spin-polarized (unrestricted) Xα scattered wave (Xα-SW) calculations on $Fe(SH)_4^{1-}$ and $Fe(SCH_3)_4^{1-}$ are in essential agreement.[15,16] The ground state of oxidized rubredoxin is high-spin $S = 5/2$; simple orbital counting arguments give a ferric d^5 Fe state for the oxidized system, and ferrous d^6 Fe in the reduced form (see our later discussion for a more precise assessment of the Fe valence state). The lowest energy spin-allowed transitions are S $\rightarrow$ Fe charge transfer, consistent with the prediction that the HOMO's are mainly S and the LUMO's are minority spin Fe levels.[15,16]

* Address correspondence to this author at the University of Washington.

(1) "Iron-Sulfur Proteins"; Lovenberg, W., Ed., Academic Press: New York, 1973; Vol. 1; *Ibid.* 1973; Vol. 2; *Ibid.* 1977; Vol. 3.

(2) Lehninger, A. L. "Biochemistry", 2nd ed.; Worth: New York, 1975; pp 488-498, 525-529, 604-606.

(3) (a) Orme-Johnson, W. H.; Davis, L. C. In ref 1, Vol. 3, pp 15-60. (b) Beinert, H. In ref 1, Vol. 3, pp 61-100. (c) Mortenson, E. L.; Nakos, G. In ref 1, Vol. 1, pp 37-64. (d) Yocum, C. F.; Seedow, J. N.; Pietro, A. S. In ref 1, Vol. 1, pp 111-127.

(4) ESR on 2-Fe proteins: Gibson, J. F.; Hall, A. O.; Thornley, J. H. M.; Watley, F. R. *Proc. Natl. Acad. Sci. U.S.A.* **1966**, *56*, 987.

(5) Magnetic Mössbauer on 2-Fe proteins: (a) Dunham, W. R.; Bearden, A. J.; Salmeen, I. T.; Palmer, G.; Sands, R. H.; Orme-Johnson, W. H.; Beinert H. *Biochem. Biophys. Acta* **1971**, *253*, 134. (b) Munck, E.; Debrunner, P. G.; Tsibris, J. C. M.; Gunsalus, I. C. *Biochemistry* **1972**, *11*, 885.

(6) Magnetic susceptibility on 2-Fe proteins: Palmer, G.; Dunham, W. R.; Fee, J. A.; Sands, R. H.; Izuka, T.; Yonetani, T. *Biochim. Biophys. Acta* **1971**, *245*, 201.

(7) Optical spectra of 2-Fe proteins: Eaton, W. A.; Palmer, G.; Fee, J. A.; Kimura, T.; Lovenberg, W. *Proc. Natl. Acad. Sci. U.S.A.* **1971**, *68*, 3015.

(8) X-ray structure of a 2-Fe protein: Tsukihara, T.; Fukuyama, K.; Tahara, H.; Katsube, Y.; Matsuura, Y.; Tanaka, N.; Kakudo, M.; Wada, K.; Matsubara, H. *J. Biochem.* **1978**, *84*, 1645.

(9) X-ray structures of 4-Fe proteins: (a) Adman, E.; Watenpaugh, K. D.; Jensen, L. H. *Proc. Natl. Acad. Sci. U.S.A.* **1975**, *72*, 4854. (b) Carter, C. W. In ref 1, Vol. 3, pp 157-204.

(10) Review of 2-Fe proteins: Sands, R. H.; Dunham, W. R. *Q. Rev. Biophys.* **1975**, *4*, 443.

(11) Magnetic susceptibility and Mössbauer of 2-Fe synthetic analogues: Gillum, W. O.; Frankel, R. B.; Foner, S.; Holm, R. H. *Inorg. Chem.* **1976**, *15*, 1095.

(12) Structure and redox properties of 2-Fe and 4-Fe analogues: (a) Mayerle, J. J.; Denmark, S. E.; De Pamphilis, B. V.; Ibers, J. A.; Holm, R. H. *J. Am. Chem. Soc.* **1975**, *97*, 1032. (b) Holm, R. H. *Acc. Chem. Res.* **1977**, *10*, 427.

(13) X-ray structure of 3-Fe protein: Stout, C. D.; Ghosh, D.; Pattabhi, V.; Robbins, A. H. *J. Biol. Chem.* **1980**, *255*, 1797. Mössbauer spectrum: Emptage, M. H.; Kent, T. A.; Huynh, B. H.; Rawlings, J.; Orme-Johnson, W. H.; Munck, E. *Ibid.* **1793**.

(14) Bertrand, P.; Gayda, J. P. *Biochem. Biophys. Acta* **1979**, *579*, 107.

(15) Hartree-Fock CI on the 1-Fe model: Bair, B. A.; Goddard, W. A., III. *J. Am. Chem. Soc.* **1978**, *100*, 5669.

(16) Spin-polarized Xα-SW on the 1-Fe model: Norman, J. G., Jr.; Jackels, S. C. *J. Am. Chem. Soc.* **1975**, *97*, 3833.

(17) Restricted Xαa-SW on the 2-Fe model: Norman, J. G., Jr.; Kalbacher, B. J.; Jackels, S. C. *J. Chem. Soc., Chem. Commun.* **1978**, 1027.

(18) (a) Restricted Xα-SW on the 4-Fe model: Yang, C. Y.; Johnson, K. H.; Holm, R. H.; Norman, J. G., Jr. *J Am. Chem. Soc.* **1975**, *97*, 6596. (b) Restricted LCAO-Xα: Geurts, P. J. M.; Gosselink, J. W.; van der Avoird, A.; Baerends, E. J.; Snijders, J. G. *Chem. Phys.* **1980**, *46*, 133.

(19) Spin-polarized Xα-SW-VB on the 2-Fe model: Norman, J. G., Jr.; Ryan, P. B.; Noodleman, L. *J. Am. Chem. Soc.* **1980**, *102*, 4279.

0002-7863/84/1506-2316$01.50/0

The initial calculations on 2(Fe–S) and 4(Fe–S) ferredoxin models were spin- and symmetry-restricted MO calculations of either Xα–SW or LCAO–Xα type.[17,18] These calculations result in a low-spin d^5 ($S = 1/2$) valence state for each Fe atom (oxidized), at a considerable loss of spin polarization energy with respect to high-spin d^5 ($S = 5/2$). Moreover, low-spin Fe is inconsistent with the presence of very low lying paramagnetic excited states in the 2(Fe–S)[19] and 4(Fe–S) systems,[10,20] with observations from X-ray photoelectron spectroscopy[21] and with a variety of Mössbauer and magnetic measurements.[10,20] It is desirable to allow for a description in which the Fe centers are both high spin, and may be ferromagnetically (both sites spin up; high spin overall) or antiferromagnetically (one site spin up, the other site spin down) coupled. An approximate but straightforward approach is to relax the total spin and spatial symmetry constraints, i.e., to perform broken symmetry UHF calculations. When this is done for 2-Fe ferredoxin models, a broken symmetry SCF wave function is found where the α-spin 3d electrons localize on one Fe and the β-spin 3d electrons localize on the opposite Fe.[19] Similar effects have been found in recent calculations on 4-Fe ferredoxin models, with two α-spin and two β-spin Fe sites.[20]

The low-spin broken symmetry state, ψ_B, is not a pure spin state, i.e., it cannot strictly be identified with the antiferromagnetic state with $S = 0$. The weights with which the pure spin states with $S = 0$ to $S = S_{max} = S_1 + S_2$ occur in ψ_B can be determined by using spin-projection techniques.[23] If the spacing between the $S_{max} + 1$ pure spin states (the Heisenberg "spin ladder") is expressed in the Heisenberg J constant, $E(S) - E(S-1) = -2JS$, the energy of ψ_B is sufficient to determine J if only one other pure spin state energy is known. This is the case for the high-spin ($S = S_{max}$) state, which can be approximated in full spatial symmetry as a single (spin-unrestricted) determinant with spins up at both sites. J is then computed from the relation:[23]

$$E(S_{max}) - E_B = -S^2_{max}J$$

This approach has been applied to 2-Fe ferredoxin models by Norman and co-workers[19] and to 4-Fe ferredoxin models by Aizman and Case.[20]

Broken symmetry and valence bond concepts are prominent in the theory of (anti)ferromagnetism through the contributions of Löwdin, Nesbet, Anderson, Hay, and others.[24] Some ionization and excitation processes are best explained by broken symmetry states or resonance structures of these;[25-28] there is an intimate connection as well between broken symmetry and electron trapping in mixed-valence compounds.[29] However, there have been few detailed ab initio calculations for antiferromagnetically coupled transition-metal complexes (aside from transition-metal diatomics) because of the size of the required CI or MC–SCF problems.[30,31] The use of broken symmetry as a direct computational tool avoids some of these problems.[19] We report below spin-polarized LCAO–Xα–VB calculations on $Fe_2S_2(SH)_4^{2-,3-}$. These are used to study the magnetic coupling of the two subunits (i.e., to determine the Heisenberg coupling constant J). A number of related experimental data—optical excitation spectra, ESR g and A tensors—have also been investigated.

Experimental Section

All calculations were made by using the Hartree–Fock–Slater program of Baerends and Ros on a CYBER 170/750 computer.[32] These programs use a combination of analytical and numerical methods to obtain a solution in LCAO form to self consistent field (SCF) equations for an Xα potential ($\alpha = 0, 7$). The calculations were made with a Slater type basis set of the form Fe 3d triple-ζ (exptl 1.40, 3.05, 6.40), Fe 3s and 3p double-ζ (exptl s 3.70, 5.80, exptl p 3.15, 5.15), Fe 4s double-ζ (exptl 1.05, 1.90), and Fe 4p single-ζ (exptl 1.50). The sulfur basis set was of double-ζ quality for S 3s (exptl 1.60, 2.60) and S 3p (exptl 1.15, 2.15); on hydrogen H 1s (exptl 0.76, 1.28), H 2p (exptl 1.00). An optimal basis set was determined by a least-squares fit to numerical Hartree–Fock–Slater results for the component atoms.[33] Hamiltonian matrix elements and the Coulomb potential are evaluated over a finite set of sample points.[32] In the present calculations, 10 400 points were used for spin-restricted D_{2h} calculations and 12 000 points for spin-polarized C_{2v} calculations (lowered space symmetry). Core orbitals were frozen but only for Fe 1s, 2s, 2p and S 1s, 2s, 2p.

The geometries for the oxidized and reduced ferredoxin models are the same as in previously published papers with one important exception.[17,19] In the present calculations, a vector from S to H will point away (H out) from rather than toward (H in) the z axis (Fe–Fe axis) as in previously published calculations. The motivation for this altered geometry lies in further Xα scattered wave calculations made subsequent to the publication of ref 19. This will be discussed in more detail in the following sections. More specifically, calculations on $Fe_2S_2(SH)_4^{2-}$, oxidized form, used a geometry (symmetry D_{2h}) with bond lengths Fe–S* = 2.21 Å, Fe–Fe = 2.69 Å, Fe–SH = 2.31 Å, and S–H = 1.34 Å and bond angles FeS*Fe = 75.0°, S*FeS* = 105.0°, SFeS = 109.5°, and FeSH = 109.5°. This model is consistent with the geometry of the oxidized synthetic analogues averaged for D_{2h} symmetry.[12,19] The structure of the reduced form is more problematical since no reduced analogue has been synthesized so that its X-ray structure could be determined. The reduced species is a Fe^{2+}/Fe^{3+} mixed-valence system. We will discuss later on the question of whether this is a system with delocalized valence or whether we are close to the localized limit.[29] We have performed calculations in a geometry consistent with trapped valence, in which the bond lengths at the reduced (Fe^{2+}) site have been adjusted according to observed trends in Fe–S bond lengths upon reduction.[19] We have taken a geometry (symmetry C_{2v}) with one Fe–S* = 2.21 Å, Fe–SH = 2.31 Å, Fe–Fe = 2.73 Å and other Fe–S* = 2.28 Å, Fe–SH = 2.38 Å. The bridge FeS*Fe = 75.0° was preserved, as were the remaining exterior bond lengths and angles (see oxidized geometry above). The Fe_2S_2* unit was taken to be planar as in the oxidized model. We have, in addition, made some calculations on the reduced form using the same geometry as in the oxidized model.

Because of the numerical sampling procedure for the required integrals, the total energy of the molecule cannot be calculated accurately. However, Ziegler's transition-state method can be used to calculate the energy of the molecule with respect to a reference state consisting of a sum of atomic or molecular fragments.[34] In our case H, S, and Fe $3d^64s^2$ atoms were taken as fragments.

(20) Spin-polarized Xα–SW–VB on the 4-Fe model: Aizman, A.; Case, D. A. *J. Am. Chem. Soc.* **1982**, *104*, 3269.

(21) Andrews, P. T.; Johnson, C. E.; Wallbank, B.; Cammack, R.; Hall, D. O.; Rao, K. K. *Biochem. J.* **1975**, *149*, 471.

(22) Compare, for example, the experimental Mössbauer quadrupole splitting with that calculated in ref 18b for 4-Fe models.

(23) Noodleman, L. *J. Chem. Phys.* **1981**, *74*, 5737.

(24) (a) Löwdin, P. O. *Rev. Mod. Phys.* **1962**, *34*, 80. *Ibid.* 520. *Phys. Rev.* **1955**, *97*, 1509. (b) Nesbet, R. K. *Phys. Rev.* **1961**, *122*, 1497. *Ibid.* **1964**, *A135*, 460. *Ann. Phys.* **1958**, *3*, 397. *Ibid.* **1958**, *4*, 87. (c) Anderson, P. W. In "Solid State Physics"; Seitz, F., Turnbull, D., Eds.; Academic Press: New York, 1963; Vol. 14, pp 99–214. *Phys. Rev.* **1959**, *115*, 2. (d) Hay, P. J.; Thibault, G. C.; Hoffman, R. *J. Am. Chem. Soc.* **1975**, *97*, 4884. (e) For a review of the literature see: Ginsberg, A. P. *Inorg. Chim. Acta Rev.* **1971**, *5*, 45.

(25) Particularly important are the theory and applications of the corresponding orbital transformation: (a) Martin, R. L. *J. Chem. Phys.* **1981**, *74*, 1852. (b) Broer-Braam, R. Ph.D. Thesis, 1981, University of Groningen, The Netherlands. (c) King, H. F.; Stanton, R. E.; Kim, H.; Wyatt, R. E.; Parr, R. G. *J. Chem. Phys.* **1967**, *47*, 1936. (d) Amos, A. T.; Hall, G. G. *Proc. R. Soc. London, Ser. A* **1961**, *A263*, 483.

(26) The relationships among broken symmetries, resonance splittings, and potential energy surfaces are carefully considered for NO_2 in: Jackels, C. F.; Davidson, E. R. *J. Chem. Phys.* **1976**, *64*, 2908.

(27) Broken symmetry and VB theory of complexes containing quadrupule metal–metal bonds: (a) Noodleman, L.; Norman, J. G., Jr. *J. Chem. Phys.* **1979**, *70*, 4903. (b) Hay, P. J. *J. Am. Chem. Soc.* **1978**, *100*, 2897. (c) Benard, M. *J. Chem. Phys.* **1979**, *71*, 2546.

(28) The literature is very extensive. For references and discussion see ref 25a,b and also: Jonkers, G.; de Lange, C. A.; Noodleman, L.; Baerends, E. J. *Mol. Phys.* **1982**, *46*, 609.

(29) From the vast literature on mixed-valence inorganic compounds and complexes, a few important papers are the following: (a) Robin, M. B.; Day, P. *Adv. Inorg. Chem. Radiochem.* **1967**, *10*, 247. (b) Allen, G. C.; Hush, N. S. *Prog. Inorg. Chem.* **1967**, *8*, 357. Hush, N. S. *Ibid.* 391. (c) Beattie, J. K.; Hush, N. S.; Taylor, P. R. *Inorg. Chem.* **1976**, *15*, 992. (d) Citrin, P. H.; Ginsberg, A. P. *J. Am. Chem. Soc.* **1981**, *103*, 3673. (e) Wong, K. Y.; Schatz, P. N. *Prog. Inorg. Chem.* **1981**, *28*, 369.

(30) An ab initio calculation of the antiferromagnetic (AF) coupling constant in copper acetate was published recently: De Loth, P.; Cassoux, P.; Daudey, J. P.; Malrieu, J. P. *J. Am. Chem. Soc.* **1981**, *103*, 4007.

(31) AF coupling in transition-metal diatomics, ref 24b and: Goodgame, M. M.; Goddard, W. W., III. *J. Phys. Chem.* **1981**, *85*, 215. *Phys. Rev. Lett.* **1982**, *48*, 135.

(32) Baerends, E. J.; Ros, P. *Int. J. Quantum Chem. Symp.* **1978**, *12*, 169.

(33) Snijders, J. G.; Vernooijs, P.; Baerends, E. J. *At. Data Nucl. Data Tables* **1981**, *26*, 483.

(34) Ziegler, T.; Rauk, A. *Theor. Chim. Acta* **1977**, *46*, 1.

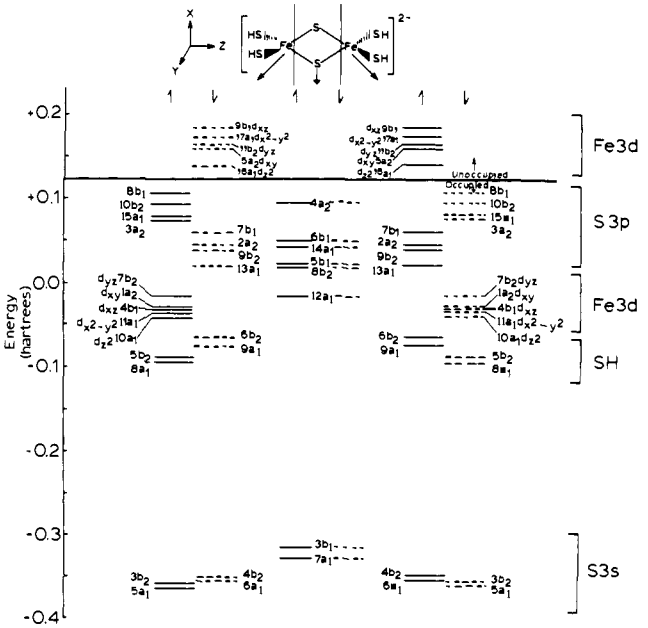

Figure 1. LCAO-Xα valence energy levels of $Fe_2S_2(SH)_4^{2-}$; AF configuration. The orbitals are grouped according to their distribution on the left, center, or right of the molecule. Spin-up levels are shown with solid lines, spin-down with dashed lines. The five occupied and five unoccupied pairs of Fe 3d orbitals are labeled.

Full-spin unrestricted SCF calculations were made for the high-spin and broken symmetry low-spin states in both oxidized and reduced forms, always in C_{2v} symmetry. Note that we always have high-spin subunits, and only use the terms high spin and low spin to denote the $S = S_{max}$ (ferromagnetic) and broken symmetry (mostly antiferromagnetic) states, respectively. In the oxidized ferredoxin, where the nuclear framework has D_{2h} symmetry, symmetry breaking has no effect in the high-spin case, but it is crucial in the low-spin case. We obtained the wave functions to very high accuracy, requiring typically 60 to 75 iterations for energy convergence. The ΔSCF energy differences, computed with Ziegler's transition-state method,[34] were used to calculate the Heisenberg exchange coupling constant J for a Heisenberg spin Hamiltonian, according to the method described in ref 23 (cf. also ref 24).

Optical excitation energies for d $\rightarrow$ d and charge-transfer transitions were calculated by the Slater transition-state method,[35] which depends on orbital eigenvalue differences. The method is accurate for one-electron excitations, and convergence was obtained in 10 to 20 iterations starting from the C_{2v} broken symmetry state. For some of the low-lying d $\rightarrow$ d states, spin contamination in the broken symmetry excited states was corrected by using additional Slater transition-state calculations for the high-spin configurations.

ESR g values and anisotropic hyperfine tensors (A tensors) were calculated by using the program of Geurts et al. with further modifications by C. Famiglietti and L. Noodleman.[36] The program requires as parameters spin-orbit coupling constants (per electron) on Fe and S, for which we have used the Fe^{2+} value ζ = 410 cm^{-1} and for S ζ = 382 cm^{-1} [37] (the Fe^{2+} spin-orbit constant may also be expressed as $\lambda = -\zeta/2S = -102.5$ cm^{-1}.[14] The nuclear g value for Fe_{57} was taken as g_N = 0.1806.[37b]

Results and Discussion

Energy Level Structure. In Figure 1, we show the energy level diagram for the broken symmetry state (low spin, $M_s = 0$) of $Fe_2S_2(SH)_4^{2-}$ in C_{2v} symmetry. As in earlier Xα scattered wave calculations,[19] the orbitals are grouped in columns according to their distribution on the left, middle, or right of the molecule and their spin. The numbering scheme is different from the Xα-SW calculations simply because we have counted the very low lying MO's (not shown in Figure 1) generated by Fe 3s, 3p atomic orbitals on the two sites: four a_1 levels, two b_1 levels, and two b_2 levels.[19,38] The basic structure of the energy level diagram and its interpretation closely follows the previous Xα-SW calculations.

The molecule consists of two high-spin subunits, each with spin vector $S = 5/2$ coupled with antiparallel alignment of the spin vectors. Due to the symmetry of the system each spin-up level is energetically degenerate with a mirror image spin-down level (for example $5a_1^{\uparrow}$ with $5a_1^{\downarrow}$, $3b_2^{\uparrow}$ with $3b_2^{\downarrow}$, $10a_1^{\uparrow}$ ($3d_{z^2}$ left) with $10a_1^{\downarrow}$ ($3d_{z^2}$ right)). The orbitals can also be grouped in up-spin/down-spin pairs that have a large overlap, i.e., still resemble doubly occupied orbitals (e.g., $10a_1^{\uparrow}$ (d_{z^2} left) and $16a_1^{\downarrow}$ (d_{z^2} left)). These pairs are in general not degenerate, but may be split due to spin polarization. This is particularly the case for the d orbitals. The occupied spin-up Fe 3d orbitals (the "magnetic orbitals") at the left are strongly stabilized, and lie considerably below the occupied S p orbitals, whereas the unoccupied 3d's lie in the virtual spectrum. The terminal S up-spin/down-spin pairs ($8b_1^{\uparrow}$–$7b_1^{\downarrow}$ and $3a_2^{\uparrow}$–$2a_2^{\downarrow}$) are also split, but much less than the d's and in the opposite sense. The S 3 p orbitals are "pushed away" by the neighboring Fe 3d orbitals with the same spin. It also turns out that the net spin density at the terminal sulfurs has the same sign as that at the adjacent Fe center. The lower lying S orbitals at the left ($5a_1$, $3b_2$) show a small stabilization of the up-spin orbitals, probably due to a slight excess up-spin density at the terminal sulfurs. The situation at the right is just the mirror image of that at the left. At the central sulfurs we find up-spin/down-spin pairs that are not split, but just constitute the degenerate mirror images. This is in agreement with the fact that the spin density at the central sulfurs is zero by symmetry.

This energy level diagram provides a clear explanation of some of the fundamental features of 2 Fe–S proteins. Upon reduction, an electron is added to $16a_1$, a localized mainly Fe $3d_{z^2}$ orbital, consistent with the large negative quadrupole splitting (QS) observed at the ferrous site by Mössbauer spectroscopy ($\Delta E_Q = -3$ mm/s, $\eta = 0$) in most ferredoxins.[5,10] In reduced spinach ferredoxin and adrenodoxin, d $\rightarrow$ d transitions are observed at about 4000 and 6000 cm^{-1}.[7,10] A further excited state of d_{xy} symmetry at about 500 to 2000 cm^{-1} above the ground state has been deduced from the temperature dependence of the Mössbauer spectrum of various proteins.[14] These observations are qualitatively consistent with spin-allowed transitions from $16a_1^{*}$ (d_{z^2}) to higher d levels. In oxidized spinach ferredoxin and adrenodoxin, optical absorption spectra are observed beginning at about 10 700 cm^{-1} (1.2 eV) and continuing to higher energy.[7,10] The first spin and dipole allowed S $\rightarrow$ Fe charge-transfer transitions begin near this low energy due to the close proximity of the sulfur HOMO's to the Fe LUMO $16a_1$. The weak overlap between the up-spin and down-spin magnetic orbitals (via the S* atoms) leads to the observed antiferromagnetic coupling, which is of superexchange type.[4-6,10,11,19]

Population Analyses. In Table I, we present a Mulliken analysis of the oxidized model charge distribution for the important occupied and virtual orbitals in terms of atomic components. (The atomic orbitals are SCF orbitals for the Fe $3d^7s^1$, S $3s^23p^4$, and H 1s atoms (spin-restricted), rather than the usual primitives.) In the occupied magnetic orbitals, the Fe 3d character is in the range 49–85%, and the spin-up orbitals are strongly localized on the left side (Fe and terminal S) of the molecule. The lowest unoccupied orbitals have from 56 to 75% Fe 3d character with the rest mainly on sulfur. In semiempirical studies of the reduced ferredoxin g tensors, the free ferrous ion Fe^{2+} spin-orbit coupling constant ζ = 400 cm^{-1} must be reduced to about ζ = 300 cm^{-1} for covalency effects to get a good fit to experiment, consistent with about 75% Fe 3d character in the LUMO's $16a_1$ to $9b_1$.[4,14] A direct calculation of the g tensors will be presented later. The high-lying sulfur HOMO's $8b_1$, $10b_2$, $3a_2$, and $15a_1$ have considerable charge on many different sulfur and iron sites. They are more delocalized than the magnetic orbitals. The net spin density at the terminal sulfurs is difficult to estimate. On the one

(35) Slater, J. C. *Adv. Quantum Chem.* **1971**, *6*, 1.
(36) Geurts, P. J. M.; Bouten, P. C. P.; van der Avoird, A. *J. Chem. Phys.* **1980**, *73*, 1306.
(37) (a) Carrington, A.; McLachlan, A. D. "Introduction to Magnetic Resonance"; Harper Int. Ed.; New York, London, Tokyo, 1969. (b) Ludwig, G. W.; Woodburg, H. H. *Phys. Rev.* **1960**, *117*, 1286.
(38) In the LCAO-Xα calculations, $Fe_2S_2(SH)_4^{2-,3-}$ ions are calculated in vacuum, without the stabilizing 2+/3+ charged sphere used in Xα-SW calculations. This accounts for the large, but constant, offset comparing the two different energy scales.

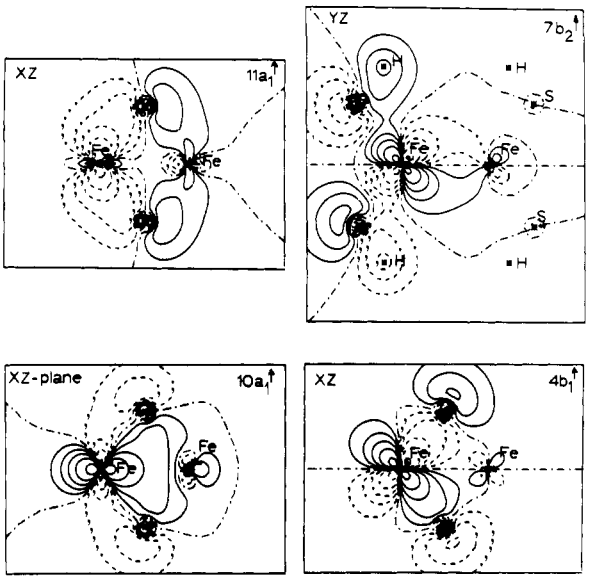

Figure 2. Contour maps for the occupied magnetic orbitals $10a_1^{\uparrow}$, $11a_1^{\uparrow}$, and $4b_1^{\uparrow}$ (plotted in xz, Fe–S* bridge plane) and $7b_2^{\uparrow}$ (plotted in yz, Fe–S terminal plane) of $Fe_2S_2(SH)_4^{2-}$. The corresponding spin-down orbitals, $10a_1^{\downarrow}$, $11a_1^{\downarrow}$, etc., are the mirror images with respect to the xy plane through bridging S. Contour values in Figures 2 and 3 are 0, ±0.02, ±0.05, ±0.10, ±0.20, and ±0.50 $(e/bohr^3)^{1/2}$.

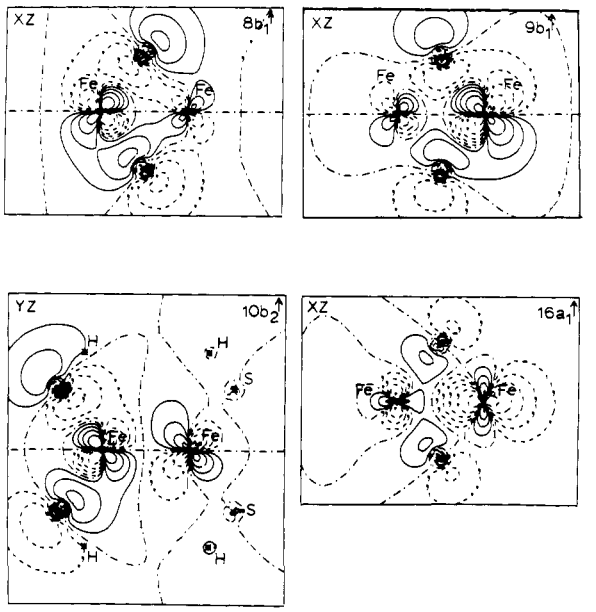

Figure 3. Contour maps for the sulfur HOMO's $8b_1^{\uparrow}$ (xz plane) and $10b_2^{\uparrow}$ (yz) and for the unoccupied Fe 3d orbitals $16a_1^{\uparrow}$ (xz) and $9b_1^{\uparrow}$ (xz) of the oxidized model $Fe_2S_2(SH)_4^{2-}$. The filled $16a_1^{\uparrow}$ of the reduced 3^- model has a very similar appearance to $16a_1^{\uparrow}$ (unoccupied).

hand, the down-spin S orbitals (left) have more weight on the terminal S than the up-spin orbitals, but on the other hand the up-spin magnetic orbital $7b_2^{\uparrow}$ shows considerable delocalization onto S (49% Fe $3d_{yz}$ and 29% S ($3s + 3p_z$) character). Also, $7b_1^{\uparrow}$ contributes 24% to S ($3p_x$, left). There turns out to be a net up-spin density (see next section).

The nature of these molecular orbitals is relevant both to the charge-transfer spectrum and to questions of electron transport. In Figure 2 we present orbital contour plots for some of the occupied Fe magnetic orbitals $10a_1^{\uparrow}$, $11a_1^{\uparrow}$, $4b_1^{\uparrow}$, and $7b_2^{\uparrow}$ illustrating the superexchange interactions in the first three and the partial S radical character in $7b_2$. Figure 3 shows plots of the two highest sulfur orbitals $8b_1^{\uparrow}$ and $10b_2^{\uparrow}$, and of $16a_1^{\uparrow}$ and $9b_1^{\uparrow}$, unoccupied Fe 3d orbitals in the oxidized model. Note the S 3p/Fe 3d bonding in the occupied spin-up magnetic orbitals (Figure 2) and antibonding in the occupied S 3p spin-up orbitals (Figure 3).

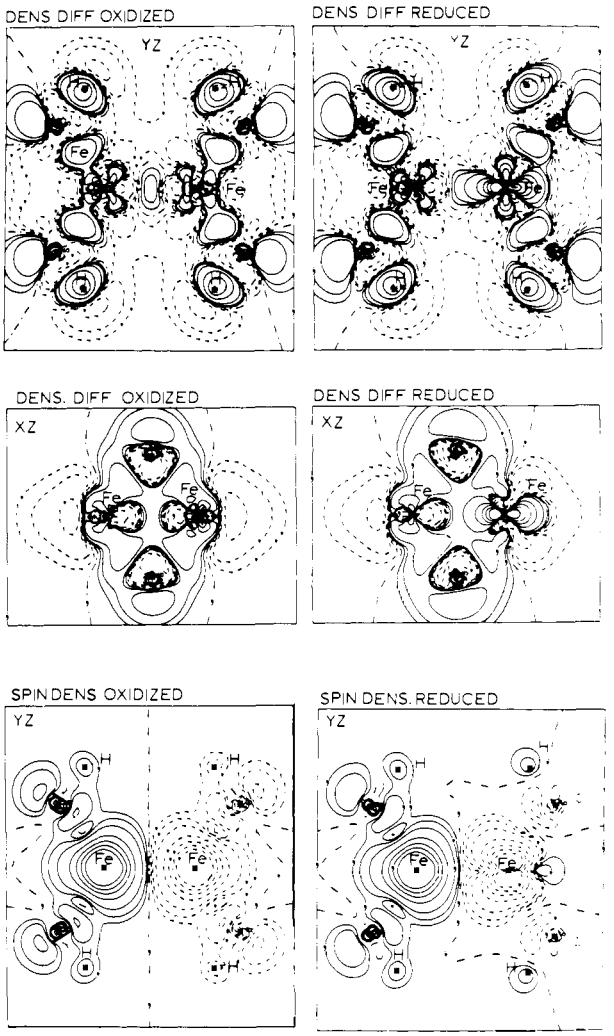

Figure 4. LCAO-Xα density difference maps (molecule minus spin-restricted atoms) and spin density maps ($\rho^{\uparrow}-\rho^{\downarrow}$) for $Fe_2S_2(SH)_4^{2-,3-}$, both oxidized and reduced forms in xz and yz planes. The reduced Fe site is at the right. Contour values are 0, ±0.001, ±0.002, ±0.005, ±0.02, ±0.05, ±0.1, and ±0.2 $e/bohr^3$ with the solid line representing a postive density difference, dashed line negative, with respect to the neutral atom fragments.

This character is reversed in the spin-down S 3p and Fe 3d orbitals (left side), cf. Figure 3. The large splitting between Fe 3d spin-up and spin-down levels due to spin polarization is thus enhanced by bonding and antibonding interactions with S 3p. Figure 4 shows density difference maps of the molecular density minus the spin-restricted atom densities (Fe $3d^64s^2$) for oxidized and reduced models $Fe_2S_2(SH)_4^{2-,3-}$ (see Experimental Section for details). Notable features are the increased densities on all sulfurs of the reduced compared with the oxidized system and a large increase in the $3d_{z^2}$ density on the reduced Fe site (at the right of the plots). These maps could be directly compared with high-precision Fourier transform data from neutron and X-ray diffraction when these become available for ferredoxins or synthetic analogues. The spin-density maps demonstrate the strong spin polarization and show the effect of reduction, i.e., adding a spin-up electron at the right side. We note that the terminal sulfurs have net S 3p spin density of the same sign as the adjacent Fe site.

Tables II and III give Mulliken analyses for the broken symmetry states of the oxidized and reduced models, respectively. On

(39) By performing separate unitary transformations on the α and β spin orbitals, it is possible to obtain new orbitals where the space part of each α orbital has nonzero overlap with precisely one β orbital, and conversely. This corresponding orbital transformation is of considerable theoretical and practical importance (see ref 25), but it is not essential for our purposes. The broken symmetry wave function is invariant to this unitary transformation.

Table I. Major Contributions (%) to Important Orbitals (see Figure 1) from Mulliken Population Analysis for $Fe_2S_2(SH)_4^{2-}$, Oxidized[a]

		H (left)	S (left)				Fe (left)			S* (middle)		
	ϵ_i, eV	1s	3s	$3p_x$	$3p_y$	$3p_z$	d_{z^2}	$d_{x^2-y^2}$	$d_{xz, yz, xy}$	$3p_x$	$3p_y$	$3p_z$
unoccupied orbitals												
$9b_1^{\downarrow}$	4.89								60	23		
$17a_1^{\downarrow}$	4.68						2	54				22
$11b_2^{\downarrow}$	4.40								64		18	
$5a_2^{\downarrow}$	4.22								73			
$16a_1^{\downarrow}$	3.75						69	6		6		4
occupied S 3p orbitals												
$8b_1^{\uparrow}$	2.86			27					15	17		25
$10b_2^{\uparrow}$ [b]	2.47				13	23			16		32	
$15a_1^{\uparrow}$ [b]	2.05				11	28		17			10	
$3a_2^{\uparrow}$	2.02			87					7			
$7b_1^{\downarrow}$ [b]	1.59			61								
$2a_2^{\downarrow}$	1.23			44					24		24	
$9b_2^{\downarrow}$	1.04					61			14			
$13a_1^{\downarrow}$ [b]	0.49				7	52						
magnetic (Fe 3d) orbitals												
$7b_2^{\uparrow}$	−0.44					20			49			
$1a_2^{\uparrow}$	−0.92								85	8		
$4b_1^{\uparrow}$	−1.01								73	15		
$11a_1^{\uparrow}$	−1.03							68				18
$10a_1^{\uparrow}$	−1.21						65			11		
HS orbitals												
$6b_2^{\downarrow}$	−1.88	32	14		36	9						
$9a_1^{\downarrow}$	−2.41	30	11		41	5						
$5b_2^{\uparrow}$	−2.44	24	7		29				32			
$8a_1^{\uparrow}$	−2.71	27	8		39	5						
S3s orbitals												
$4b_2^{\downarrow}$	−9.61	24	69									
$6a_1^{\downarrow}$	−9.74	22	64									
$3b_2^{\uparrow}$	−9.75	21	71									
$5a_1^{\uparrow}$	−9.90	19	65									

	ϵ_i	S 3p (left)	Fe 3d (left)	S* 3p	Fe 3d (right)	S 3p (right)
S* $3p_x$ orbitals						
$4a_2^{\uparrow}$	2.49			48		44
$6b_1^{\uparrow}$	1.24	25		26	23	15
$14a_1^{\uparrow}$	1.07		15	35	20	11
$5b_1^{\uparrow}$	0.63	15		52		
$8b_2^{\uparrow}$	0.52	35		34		7
$12a_1^{\uparrow}$	−0.47	28		37		

[a] For each spin-up (down) orbital there is a degenerate spin-down (up) partner, which is the spatial mirror image of the one given in the table. [b] A number of orbitals also have some amplitude at the right side of the molecule: $10b_2^{\uparrow}$: 10% $3d_{yz}$ Fe (right). $15a_1^{\uparrow}$: 14% $3d_{z^2}$, 10% $3d_{x^2-y^2}$ Fe (right). $7b_1^{\downarrow}$: 24% $3p_x$ S (right). $13a_1^{\downarrow}$: 9% $3d_{z^2}$ Fe (right).

Table II. Mulliken Population Analysis for $Fe_2S_2(SH)_4^{2-}$, Oxidized

(A) Fe 3d Populations

	spin α		spin β		total (α + β) spin pop. (α − β)	
	Fe(left)	Fe(right)	Fe(left)	Fe(right)	Fe(left) (= right)	Fe(left) (= −right)
a_1 $3d_{z^2}$	0.97	0.25	0.23	0.98	1.21	0.74
$3d_{x^2-y^2}$	0.95	0.37	0.38	0.95	1.33	0.57
a_2 $3d_{xy}$	0.99	0.27	0.27	0.99	1.26	0.72
b_1 $3d_{xz}$	0.98	0.39	0.39	0.97	1.36	0.59
b_2 $3d_{yz}$	0.99	0.34	0.35	0.99	1.33	0.64
total 3d	4.87	1.62	1.62	4.88	6.49	3.25

(B) Total Fe and S Populations

	Fe(left)	Fe(right)	S*	S(left)	S(right)	H(left)	H(right)
spin α	9.78	6.20	3.09	3.13	2.98	0.65	0.66
spin β	6.25	9.74	3.09	2.97	3.13	0.63	0.68
total pop. (α + β)	16.03	15.94	6.18	6.10	6.10	1.29	1.35
spin pop. (α − β)	+3.53	−3.54	−0.005	+0.16	−0.15	+0.02	−0.02

the Fe sites, a breakdown into the different Fe 3d components is shown. In the oxidized model, the Fe 3d spin population is 3.25 electrons, the total Fe spin population is 3.54, and the total Fe 3d population is 6.49. On the terminal S, the spin population is 0.15 per site or 0.30 for 2 S. While the energy level diagram is the expected one for Fe^{3+} d^5 sites, the detailed spin and charge distribution are closer to d^6 than to ferric d^5, and the terminal sulfur spin population is substantial. For comparison, if one unpaired electron were spread over the four sulfur ligands adjacent to one Fe site, the spin population on the two terminal sulfurs

Table III. Mulliken Population Analysis for $Fe_2S_2(SH)_4^{3-}$, Reduced[a]

(A) Fe 3d Populations

	spin α		spin β		total (α + β)		spin pop. (α − β)	
	Fe(left)	Fe(right)	Fe(left)	Fe(right)	Fe(left)	Fe(right)	Fe(left)	Fe(right)
a_1 $3d_{z^2}$	0.98	0.91	0.22	0.95	1.19	1.86	0.76	−0.04
$3d_{x^2-y^2}$	0.97	0.28	0.35	0.96	1.32	1.23	0.62	−0.68
a_2 $3d_{xy}$	0.99	0.15	0.28	0.99	1.27	1.14	0.71	−0.84
b_1 $3d_{xz}$	0.98	0.24	0.39	0.96	1.37	1.21	0.59	−0.72
b_2 $3d_{yz}$	0.99	0.16	0.33	0.99	1.32	1.15	0.66	−0.83
total 3d	4.91	1.75	1.57	4.85	6.48	6.60	3.34	−3.10

(B) Total Fe and S Populations

	Fe(left)	Fe(right)	S*	S(left)	S(right)	H(left)	H(right)
spin α	9.78	6.19	3.34	3.17	3.12	0.66	0.72
spin β	6.16	9.55	3.07	3.06	3.18	0.64	0.69
total (α + β)	15.94	15.74	6.41	6.23	6.30	1.31	1.41
spin pop. (α − β)	+3.62	−3.35	+0.27	+0.11	−0.06	+0.02	+0.02

[a] To form the reduced model from the oxidized, one electron of spin α is placed in orbital $16a_1^{\uparrow}$ of the broken symmetry wave function (AF configuration). The reduced site, Fe(right), has all Fe-S bonds lengthened by 0.07 Å; the oxidized site Fe(left) is unchanged.

Table IV. Population and Spin Density Differences Reduced minus Oxidized Model

	Fe(left)	Fe(right) (reduced site)	S*	S(left)	S(right)	H(left)	H(right)
change in							
total pop. (α + β)	−0.09	−0.20	+0.23	+0.13	+0.20	+0.02	+0.07
spin pop.[a] (α − β)	+0.09	+0.19	+0.27	−0.05	+0.09	+0.002	+0.04
	(inc)	(dec)	(inc)	(dec)	(dec)	(inc)	(inc)
total 3d pop.	−0.04	+0.106					
3d spin pop.[a]	+0.091	+0.157					
	(inc)	(dec)					

[a] The sign of the spin population difference reduced − oxidized does not indicate whether the absolute magnitude of the spin density decreased or increased, as this depends on the sign of the initial spin density. Therefore increase (inc) or decrease (dec) is explicitly noted.

would be 0.50. In earlier calculations with Xα–VB–SW, partial sulfur radical character was also found.[19] In the HF–CI calculations of Bair and Goddard on oxidized rubedoxin models, $Fe^{2+}(d^6)$–S· terms have the highest weight (80% in the CI wave functions).[15]

It should be emphasized that the spin density in Table II for the oxidized model is not observable in the $S = 0$ ground state. Mathematically, upon projection of the totally symmetric $S = 0$ state out of the broken symmetry state, the spin density vanishes. The higher states ($S > 0$) of the spin ladder have nonvanishing spin density as shown by proton NMR on oxidized proteins (at the cysteine methylene protons) and on synthetic analogues.[10,11] In principle, the observed spin density at the protons for $S > 0$ can be related to that in the broken symmetry by spin projection, or more simply, by use of the vector model of Gibson.[4,10] We will not pursue this topic any further here since our theoretical model cluster is too small to include the required R groups.

We now consider the charge and spin-density distribution in the reduced model (Table III). In Table IV, we compare these total charge and spin densities with the corresponding ones for the oxidized model. The most dramatic difference is in the distribution of the Fe 3d electrons (Tables II and III), as expected from the orbital description of the reduction. While in the oxidized system the Fe 3d charge distribution is nearly isotropic on both sites, in the reduced there is a large increase (0.64 e^-) in the reduced site Fe $3d_{z^2}$ population; the differences on the oxidized Fe site (left) are much smaller. There are some surprises, however, when we compare the total atom populations on Fe and S, or the total Fe 3d population (Table IV). The total Fe 3d population on the reduced site increases by only 0.11 e^- compared with the oxidized model. Moreover, there is a net *decrease* in the total electronic charge at both Fe sites and a large increase distributed over all the sulfur sites. When one electron is added to $16a_1^{\uparrow}$ (Fe $3d_{z^2}$), there are large relaxation effects in the passive orbitals on both sulfur and Fe. The increased charge in the reduced form goes almost entirely to S, S*. On the reduced Fe site, the new charge density is highly anisotropic and the Fe 3d population shows a modest increase. Although the overall charge distribution is surprising at first sight, there is a good deal of supporting evidence for such charge rearrangement in many transition-metal complexes. Again these results are consistent with the HF–CI results on rubedoxin, where 80% of the charge increase upon reduction goes to the four sulfurs.[15] In a theoretical study by LCAO–Xα of tetrahedral transition-metal oxide complexes, it was found that upon reduction most of the added charge migrates to the ligands, while the active orbital is mainly metal.[40] Similar charge rearrangements were found in L → M charge-transfer excited states of these complexes. For Fe–S proteins, the important point is that both the Fe and sulfur centers are intimately involved in the redox behavior.[41]

Some other results in Table IV are also of interest. There is a small asymmetry between the left and right sides of the molecule in total charge with 2 (SH) (right) adjacent to the reduced Fe site, exceeding 2 (SH) (left) by 0.24 e^-. This may promote greater hydrogen bonding by the cysteine sulfurs at the reduced than at the oxidized site in reduced ferredoxin proteins. As expected, the increased charge on all sulfurs in the reduced form (compared with the oxidized protein) will strengthen available N–H···S hydrogen bonds.[9] (X-ray analysis of chloroplast ferredoxin shows N–H···S hydrogen bonding to cysteine sulfur but not to bridging sulfur[8].)

Heisenberg Coupling Constants. In previous work we developed the theory relating the Heisenberg exchange coupling constant J to the energies of the broken symmetry (low-spin) state E_B and the high-spin state $E(S_{max})$.[23] For the oxidized system, the broken symmetry state (to which we will also refer as *low spin* and

(40) Ziegler, T.; Rauk, A.; Baerends, E. J. *Chem. Phys.* **1976**, *16*, 209.
(41) Recent studies of Fe–S protein reactions with aquated electrons suggest involvement of cysteine sulfur in electron transfer, consistent also with structural studies of 2(Fe–S) ferredoxins showing that cysteine sulfur is exposed to the solvent. (a) Adzamli, I. K.; Kim, H. O. W.; Sykes, A. G.; Buxton, G. V. *J. Inorg. Biochem.* **1982**, *16*, 311. (b) Fukuyama, K.; Hase, T.; Matsumoto, S.; Tsukihara, T.; Katsube, Y.; Tanaka, N.; Kakudo, M.; Wada, K.; Matsubara, H. *Nature (London)* **1980**, *286*, 522.

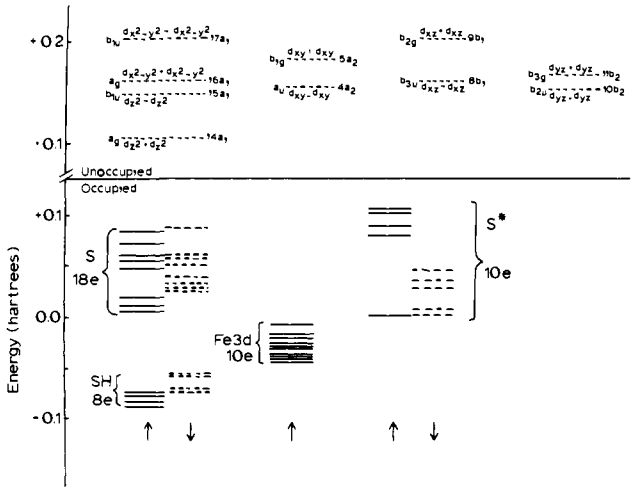

Figure 5. Energy levels for the high-spin F configuration of $Fe_2S_2(SH)_4^{2-}$. Again spin-up levels are shown with solid lines, spin-down with dashed lines. There is an excess of 10 spin-up electrons. The low-lying unoccupied levels are all spin-down Fe 3d, and their symmetries are specified both in C_{2v} and D_{2h} point groups. The calculations were actually made in the C_{2v} symmetry, but this has hardly any effect. The Fe 3d levels in the virtual spectrum have been grouped according to the irreducible representation of C_{2v}. The occupied spectrum is grouped according to orbital character (S, Fe, etc.), not symmetry.

antiferromagnetic) is described in Figure 1. For future reference, the occupation scheme for this antiferromagnetic (AF) configuration has all orbitals filled through $(15a_1)(4a_2)(8b_1)(10b_2)$ (α and β spin). The oxidized high-spin state (or ferromagnetic (F) configuration) is occupied through $(17a_1)(5a_2)(9b_1)(11b_2)$ (α spin) and $(13a_1)(3a_2)(7b_1)(9b_2)$ (β spin). This F state has $S = S_{max} = 5$ with 10 spin α magnetic electrons and 0 spin β; its energy level diagram, derived from an independent SCF calculation for $S = 5$, is given in Figure 5. Although in principle the F state could be calculated in D_{2h} symmetry, we have used C_{2v} instead to maintain comparability with the C_{2v} broken symmetry calculation. The energy difference between the (symmetric) F and (broken symmetry) AF states is related to the Heisenberg exchange coupling constant J by[23]

$$E(S_{max}) - E_B = -S_{max}^2 J \quad (1)$$

There are $S_{max} + 1$ different pure spin states having relative energies $E(S) - E(S-1) = -2JS$ for $S_{max} \geq S \geq 0$.[24] The singlet–triplet splitting is $2J$. The energy difference between $\psi(S_{max})$ and the singlet ground state is

$$E(S_{max}) - E(S=0) = -S_{max}(S_{max}+1)J \quad (2)$$

so the singlet has energy $E_B + S_{max}J$, or $5|J|$ below the broken symmetry energy. J can be calculated from eq 1 and used to determine all $E(S)$.

When this procedure is used, we calculate $J = -310$ cm^{-1} for the oxidized model. The previously reported J value from Xα–SW–VB was $J = -265$ cm^{-1}.[19] As noted in the Experimental Section, the present geometry differs from that used in the previous paper (by 180° rotation of all S–H bonds about the respective Fe–S axes, all Fe–SH angles are 109.5° as previously). With the present geometry, Xα–SW–VB predicts $J = -303$ cm^{-1},[42] so the results by the two different Xα methods are highly consistent. Experimentally, $J = -183$ and -149 cm^{-1}, for oxidized spinach ferredoxin[6] and synthetic analogue,[11] respectively. In oxidized adrenodoxin, magnetic susceptibility[43] and resonance Raman[44] measurements give J more negative than -350 cm^{-1} and $J = -497$ cm^{-1}, respectively. The lower values, $J = -183, -149$ cm^{-1}, are probably more typical for most 2-Fe ferredoxins, so that the theoretical J value is only qualitatively correct. The relevant energy differences are very small so that discrepancies of this size between theory and experiment are not unexpected (cf. ref 30). It is helpful for the accuracy of the theoretical J value that J is computed from eq 1, since the error in J is only $1/S_{max}^2 = 1/25$ that of the energy difference $E(S_{max}) - E_B$.[23] An accurate, direct calculation of J would be far more difficult.

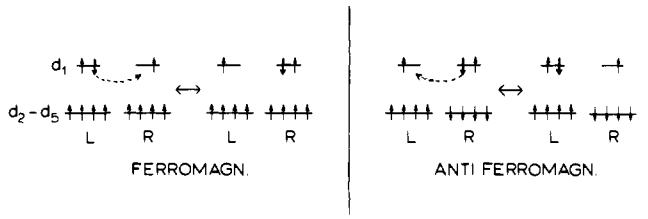

Figure 6. Delocalization of the added electron (reduced species) in the ferromagnetic (F) and antiferromagnetic (AF) configuration: there is loss of spin polarization energy for AF but not for F.

Calculating J for the reduced system is more complicated. For reasons of space, we will relegate the detailed mathematical analysis to the Appendix. We can only give a brief physical argument here. Adding an electron to orbital $16a_1^{\uparrow}$, i.e., to Fe d_{z^2} at the right, yields a formally Fe^{3+}/Fe^{2+} mixed-valence system.[29] The AF configuration has the wave function (with $d_1 = d_{z^2}$)

$$\psi_R(B) = N^{-1/2}|(\text{rest})\ d_1^L\alpha\bar{d}_2^L\alpha \ldots \bar{d}_5^L\alpha;\ (d_1^R\alpha\bar{d}_1^R\beta)\bar{d}_2^R\beta \ldots \bar{d}_5^R\beta| \quad (3)$$

where the unbarred d-like orbitals are orthogonal, $\langle d_i^L|d_j^R\rangle = 0$, but where the magnetic orbitals $\bar{d}_i$ are overlapping (see ref 23)

$$\bar{d}_i^L = d_i^L + c_i d_i^R;\ \bar{d}_i^R = d_i^R + c_i d_i^L \quad (4)$$

$$\langle d_1^L|\bar{d}_1^R\rangle = c_1$$

$$\langle \bar{d}_i^L|\bar{d}_i^R\rangle = c_i \text{ for } i = 2\text{–}5$$

The coefficients are of two types; c_i for $i = 2$–5 lead upon spin projection of the broken symmetry state $\psi_R(B)$ to a Heisenberg Hamiltonian for the reduced system. By contrast, c_1 represents the extent of delocalization in the 3-electron bond $d_1^L\alpha d_1^R\alpha\bar{d}_1^R\beta$, with $c = c_1 = \pm 1$ giving complete delocalization, and $c = 0$ complete localization (or trapped valence). Analysis of the $3d_{z^2}$ charge distribution on Fe (right) and Fe (left) in Table III yields an approximate delocalization coefficient $c = 0.48$ in the trapped valence range. In contrast to the spontaneous symmetry breaking and localization we find in the AF configuration, in the ferromagnetic configuration the added electron delocalizes over the two centers (it goes into $d_{1g} = (d_{z^2}^L + d_{z^2}^R)$, $14a_1^{\downarrow}$ in the level diagram of Figure 5, or at higher energy into $d_{1u} = (d_{z^2}^L - d_{z^2}^R) = 15a_1^{\downarrow}$), and we do not find symmetry breaking.

We can understand this difference between the F and AF configurations when we realize that in the F configuration delocalization does not imply loss of spin polarization, whereas in AF it does. This is schematically illustrated in Figure 6. In the F case, delocalization implies mixing two equivalent left/right determinants, but in the AF case delocalization can only occur by mixing in a determinant that is less stabilized by spin polarization. For AF, the symmetry breaking is clearly driven by the spin polarization energy. (Symmetry breaking can also result from electronic polarization, as found in the PES of some binuclear complexes.[45–47] This mechanism is incompatible with the energy

(42) Norman, J. G.; Osborne, J.; Noodleman, L., unpublished calculations made subsequent to ref 19.
(43) Palmer, G. In ref 1, Vol. 2, pp 285–325.
(44) Resonance Raman on adrenodoxin: (a) Adar, F.; Blum, H.; Leigh, J. S., Jr.; Ohnishi, T.; Salerno, J. *FEBS Lett.* **1977**, *84*, 214. On spinach ferredoxin: (b) Blum, H.; Adar, F.; Salerno, J. C.; Leigh, J. S., Jr. *Biochem. Biophys. Res. Commun.* **1977**, *77*, 650.
(45) Upton, T. H.; Goddard, W. A., III. *J. Am. Chem. Soc.* **1978**, *100*, 5659.
(46) (a) Van Dam, H.; Stufkens, D. J.; Oskam, A. *J. Electron Spectrosc. Relat. Phenom.* **1980**, *21*, 47. (b) Van Dam, H.; Louwen, J. N.; Oskam, A. *Ibid.* **1980**, *21*, 57.
(47) (a) Post, D.; Baerends, E. J. *Chem. Phys. Lett.* **1982**, *86*, 176. (b) Cox, P.; Bénard, M.; Veillard, A. *Ibid.* **1982**, *87*, 159. (c) Newton, M. D. *Ibid.* **1982**, *90*, 291. (d) Messmer, R. P.; Caves, T. C.; Kao, C. M. *Ibid.* **1982**, *90*, 296.

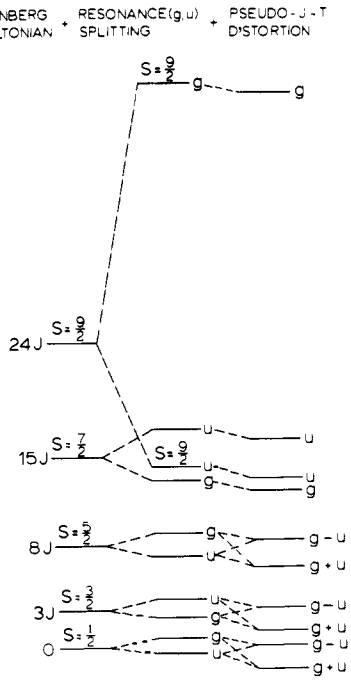

Figure 7. Schematic diagram for the Heisenberg spin ladder of a reduced ferredoxin dimer, assumed to be initially in a symmetric D_{2h} geometry, in the presence of resonance (g, u) splitting and vibronic (or environmental) coupling, g = A_g, u = B_{1u}. For $S = 9/2$, g = $^{10}A_g = {}^{11}B_{1u} \times {}^2b_{1u}$ and u = $^{10}B_{1u} = {}^{11}B_{1u} \times {}^2a_g$.

level structure for F and AF states.)

The argument above for the AF configuration is incomplete for two reasons. (1) The correct physical states are pure spin states $\psi(S)$ and (2) $\psi(B)$ and $\psi(S)$ are clearly asymmetric even in a symmetric (D_{2h}) geometry; no proper state function can have this property. Therefore, consider adding one electron to $16a_1^{\downarrow}$ and then interchanging all $\alpha \rightleftarrows \beta$ spins to form $\psi_L(B)$, the mirror image of $\psi_R(B)$. Spin projection[23] produces the pure spin functions $\psi_L(S) = N(S)^{-1/2}O(S, M = 1/2)\psi_L(B)$ with $N(S)^{-1/2}$ a normalization constant (similarly for $\psi_R(S)$). When the molecule has D_{2h} symmetry, each electronic state has definite g or u symmetry under inversion: $\psi_{g,u}(S) = \psi_L(S) \pm \psi_R(S)$ (and $\psi_{g,u}(B) = \psi_L(B) \pm \psi_R(B)$). The effect is presented schematically in Figure 7. Superimposed on the Heisenberg spin ladder are resonant g, u splittings $\Delta E_{g,u}(S)$ determined by the Hamiltonian matrix element $H_{LR} = \langle\psi_L(S)|H|\psi_R(S)\rangle$. To low order in perturbation theory, H_{LR} and $\Delta E_{g,u}$ are proportional to $(S + {}^1/_2)$; see the Appendix. By direct calculation (see Figure 5), for $S = S_{max} = {}^9/_2$ and $\Delta E_{g,u}$ = 0.64 eV. Therefore, for $S = 1/2$, $\Delta E_{g,u}$ is only of the order of 0.1 eV. One expects that the system is susceptible to a pseudo Jahn–Teller distortion for $S = 1/2$ (or small S), and also that other environmental asymmetries (for example, from the protein environment) will lead to a localized mixed-valence complex. In reduced 2-Fe ferredoxin proteins, strong evidence for trapped valence is found in the appearance of two quadrupole doublets (an inner pair and an outer pair) in the Mössbauer spectrum.[5,10]

The magnetic coupling equation is most easily defined when the ψ_L/ψ_R interaction is absent or when localized states are produced by the various asymmetries discussed above. When the two different Fe^{3+}/Fe^{2+} monomers, with $S_1 = n/2$ and $S_2 = n - 1/2$, respectively ($n = 5$), are spin coupled eq 36 and 37 of ref 23 can be simplified[48] to give

$$E(S_{max}) - E_B = -n(n-1)J \quad (5)$$

$$E(S_{max}) - E(S = 1/2) = -(n+1)(n-1)J \quad (6)$$

Here E_B is the energy of the broken symmetry AF configuration $E_B = \langle\psi_R(B)|H|\psi_R(B)\rangle$ and $E(S_{max})$ is the energy of the wave function corresponding to ferromagnetic coupling of $\vec{S}_1$ and $\vec{S}_2$, obtained from $\psi_R(B)$ by spin projection $\psi_R(S_{max}) = N^{-1/2}O(S_{max})\psi_R(B)$. After some analysis, one can show that $\psi_R(S_{max})$ has energy (see the $S = 9/2$ state of the Heisenberg ladder in Figure 7)

$$E(S_{max}) = \frac{1}{2}(E_g + E_u) + \frac{c}{1+c^2}(E_g - E_u) \quad (7)$$

where E_g and E_u are the energies of the ferromagnetic states with the added electron in d_{1g} and d_{1u} ($14a_1^{\downarrow}$, $15a_1^{\downarrow}$), respectively. From eq 5 and 7 and with $c = 0.48$, we obtain $J = -73$ cm^{-1}; if a completely localized wave function were assumed ($c = 0$), eq 5 and 7 give $J = -173$ cm^{-1}. Experimental J values for reduced ferredoxin are -98^{+5}_{-10} cm^{-1} from blue green algae[49] and -110 cm^{-1} from spinach[43] based on magnetic susceptibility measurements. Given the approximation in our analysis, and the sensitivity of the calculated J to the delocalization coefficient, the agreement with experiment is satisfactory.

Returning to the issue of the resonant g, u splittings $\Delta E_{g,u}(S)$, for sufficiently large $\Delta E_{g,u}$, the system will remain essentially delocalized despite small environmental asymmetries. This is the expected behavior for the high-spin $S = 9/2$ states with energies E_g and E_u (Figure 7), since $\Delta E_{g,u}$ = 0.64 eV is fairly large. The observed valence state of oxidized bacterial ferredoxin and its synthetic analogues, $Fe_4S_4(SR)_4^{2-}$, is quite interesting in this context. Although the 2^- state has a formal valence of $2Fe^{2+} + 2Fe^{3+}$, Mössbauer spectroscopy shows four equivalent $Fe^{2.5+}$ sites.[50,51] This is consistent with an internally delocalized $S = 9/2$ spin state for each dimeric 2(Fe–S) subunit.[20,51] Very recently, Aizman and Case have performed Xα–VB–SW calculations on the bacterial ferredoxin model system $Fe_4S_4(SCH_3)_4^{2-}$. The results show antiferromagnetic coupling between two delocalized high-spin ($S = 9/2$) 2(Fe–S) subunits with a predicted Heisenberg exchange constant of -190 cm^{-1}, compared with $J = -230$ cm^{-1} in synthetic model compounds.

State Energies, Bond Energies, and Redox Potential. All state energies were determined with respect to spin-polarized S, H, and $Fe(3d^64s^2)$ atoms. For the oxidized model, the broken symmetry energy is $E_B(ox) = -37.52$ eV, the singlet energy $E(S = 0) = -37.71$ eV, and the high-spin energy $E(S = 5) = -36.56$ eV. The spin- and symmetry-restricted D_{2h} solution, corresponding to two low-spin $S = 1/2$ Fe sites, has energy $E(D_{2h}) = -32.96$ eV, 4.6 eV above the broken symmetry solution, and 3.6 eV above the ferromagnetic high-spin state. The effect of spin polarization is clearly very large. From the energy of 4 SH bonds,[52] 14.4 eV, the computed Fe–S bond strength is 2.91 eV (67.2 kcal/mol), with 8 Fe–S bonds in the complex. The strength of a single Fe–S bond has not been determined experimentally in proteins or related Fe–S compounds.[53]

For the reduced ion $E_B(red.) = -31.28$ eV and the ground-state energy $E(S = 1/2) = E_B(red.) + 4J = -31.32$ eV (for $E(S = 9/2, {}^{10}B_{1u}) = -31.16$ eV). Then the ionization energy of the reduced ion IP = 6.39 eV. The IP of the reduced ion gives the standard redox potential E^0 when corrected for the difference in solvation energy ΔU between the oxidized and reduced systems and referenced to a standard H electrode ΔSHE = −4.5 eV.[15] To evaluate ΔU, we have assumed a spherical cavity field of radius r_0 = 3.9 Å[54] and used $\epsilon = 37$, the dielectric constant for the solvent DMF,[15] giving $\Delta U = +8.96$ eV. The calculated redox potential is E^0 (theory) = IP + ΔU + ΔSHE = −1.92 eV. The corresponding

(48) Liechtenstein, A., personal communication with L.N.

(49) Petersson, L.; Cammack, R.; Rao, K. K. *Biochim. Biophys. Acta* **1980**, *622*, 18.

(50) (a) Holm, R. H.; Ibers, J. A. In ref 1, Vol. 3, pp 206–281. (b) Cammack, R.; Dickson, D. P. E.; Johnson, C. E. In ref 1, Vol. 3, pp 283–330.

(51) Dickson, D. P. E.; Johnson, C. E.; Thompson, C. L.; Cammack, R.; Evan, M. C. W.; Hall, D. O.; Rao, K. K.; Weser, U. *J. Phys. (Paris)* **1974**, *35*, C6-343.

(52) Cotton, F. A.; Wilkinson, G. "Advanced Inorganic Chemistry", 3rd ed.; Interscience: New York, 1972; p 113.

(53) Hoggins, J. T.; Steinfink, H. *Inorg. Chem.* **1976**, *15*, 1682.

(54) The spherical volume enclosed by r_0 is about the same as the volume of a rectangular solid enclosing the $Fe_2S_2(SH)_4^{2-}$ ion. The entire S* and S atoms are included, as are the H nuclei (the latter form the $\pm y$ boundaries).

Table V. g and A Tensors for Reduced Ferredoxin from the Vector Coupling Model

(A) LCAO-Xα Calculations

	g site tensors		total g tensors $g = (7/3)g_1 - (4/3)g_2$
	ferrous: g_2	ferric: g_1	
	g Tensor		
g_x	2.118	2.010	1.866
g_y	2.038	2.005	1.962
g_z	2.005	2.005	2.006
	actual A tensors (in MHz)		
	ferrous	ferric	
A_x	+9.108	−1.425	
A_y	+3.952	+1.031	
A_z	−13.061	+0.394	

(B) Experimental[a]

	reduced spinach ferredoxin		reduced putidaredoxin	
	g Tensors			
g_x	1.88		1.94	
g_y	1.96		1.94	
g_z	2.04		2.02	
	A tensors			
	ferrous	ferric	ferrous	ferric
A_x	+7.5	−1.6	+7.0	−2.7
A_y	+3.2	−0.7	+1.8	−0.1
A_z	−10.7	+2.3	−8.8	+2.9
a	−15.8	−20.3	−17.5	−21.3

[a] For spinach ferredoxin, Dunham et al., ref 5a; for putidaredoxin, Munck et al., ref 5b. Also see Sands and Dunham, ref 10.

experimental values are −0.24 to −0.43 eV in various proteins and −1.09 to −1.49 eV in synthetic analogues.[12] It is sensible that E^0 for $Fe_2S_2(SH)_4^{2-,3-}$ is more negative than the experimental values above since the relevant ion is smaller, and from basic electrostatics, the internal electron–electron repulsion upon reduction will increase more rapidly with decreasing size than will the compensating cavity field term. A proper quantitative theory would require using the theory of Westheimer and Kirkwood[55] to obtain the cavity field correction for an ellipsoidal rather than a spherical cavity and accounting for the size of the complex and the polarizability of the R groups.

$\vec{g}$ and $\vec{A}$ Tensors. Table V compares our calculated g and A tensors with the experimental values for reduced spinach ferredoxin and reduced putidaredoxin.[4,5,10] When the program of Geurts et al.[36] was used, we computed internal g and A tensors for the ferrous and ferric sites from the low-spin broken symmetry wave function for $Fe_2S_2(SH)_4^{3-}$. The resulting internal g and A tensors (the g-site tensors and actual A tensors in Table V) are recoupled according to Gibson's vector model[4,5,10] to give the total effective g tensor $g_i = 7/3g_{1i} - 4/3g_{2i}$ (i = x, y, z) and the effective A tensors $A_{1\text{eff}} = 7/3\ A_1$ and $A_{2\text{eff}} = -4/3\ A_2$ where A_1 and A_2 are the actual A tensors for the ferric and ferrous sites, respectively (similarly for g_1 and g_2). We report the actual A tensors only, and for the experimental values we have separated out the isotropic term, $a = a_F$(Fermi contact) + a_{SO}(spin orbit). In order to properly calculate the Fermi contact term, the spin polarization of the Fe core must be included, so we cannot give a theoretical value. Even with a spin-polarized core, Xα theory is often deficient for determining the Fermi contact coupling in high-spin atoms.[56]

Comparing experimental and theoretical values, the LCAO–Xα results agree better overall with the reduced spinach ferredoxin results than with reduced putidaredoxin results,[5,10] the deciding factor being the much better agreement of the g tensors. The theoretical ferrous A tensors are in reasonable agreement with both types of experimental A tensors, but the ferric A tensors agree poorly with experiment. The calculations used all single excitations out of the occupied $16a_1^{\uparrow}$ level (of which only the low-lying d → d excitations turn out to be important) and all single excitations into the empty $16a_1^{\downarrow}$ level (see Figure 1). One problem is that the experimental error bars for the A tensors (on both sites) are large, particularly compared to the small magnitude of the ferric A tensor (anisotropic part). Our theoretical treatment of the ferric site A tensor is also deficient, and this is probably a more serious problem. According to McGarvey,[57] it is necessary to consider excitations into other low-lying empty d levels ($5a_2^{\downarrow}$ through $9b_1^{\downarrow}$) and perhaps higher order excitations as well for the ferric d^5 site, accounting for the poor agreement of the ferric A tensors with experiment.

The vector model as it is usually used includes only Fe site terms, and the question arises whether sulfur contributions have any effect on the g and A tensors. Although the sulfur ligands were explicitly included in our theoretical model, the results were nearly the same as those obtained from the Fe terms alone. By contrast, the effects of Fe–S covalency (decreasing the Fe orbital coefficients) are very important. These were taken into account directly from the covalency inherent in the broken symmetry wave function.

The picture that emerges from our g and A tensor calculations is closely related to the semiempirical analysis of Bertrand and Gayda.[14] They showed that g tensor and A tensor data in a variety of proteins could be correlated by using a ligand field model. The principle ingredients in the model are the spin-orbit coupling constant, the d → d excitation energies on the ferrous site, and the mixing between $3d_{z^2}$ and $3d_{x^2-y^2}$ for the minority spin orbital on ferrous Fe($16a_1^{\uparrow}$) in the reduced system. The mixing parameter θ is defined by $|\phi_0\rangle = |16a_1^{\uparrow}\rangle = \cos\theta|d_{z^2}\rangle + \sin\theta|d_{x^2-y^2}\rangle$ and largely accounts for the variation in g values among different proteins. $\theta = 0°$ represents a purely axial d_{z^2} orbital for the added electron. For our theoretical model, we calculate $\theta = +8°$; the resulting g tensors correspond closely with spinach ferredoxin. Bertrand and Gayda suggest that θ lies between 0 and −18° for all 2-Fe proteins, but this result depends on assuming a highly anisotropic ferric g_1 tensor. For our more isotropic g_1 tensor, θ is usually positive.

Previous Xα–SW–VB calculations (some unpublished)[42] showed that θ depends on the orientation of SH groups in the $Fe_2S_2(SH)_4^{3-}$ model. This is equivalent to a dependence on the S-cysteine bond orientation about the Fe–S axis in the proteins; Xα–SW–VB[19] predicts $\theta = +24.5°$ for all SH groups pointing toward $\hat{z}$ (C_{2v} molecular symmetry) and $\theta = +13.5°$ for all SH away from $\hat{z}$. The latter value (based on unpublished calculations)[42] compares well with the LCAO results $\theta = 8°$ in the same geometry. The Xα–SW calculations were used as a guide for choosing a sensible geometry for the present LCAO–Xα work. A close comparison of our Figure 1 with Figure 1 in ref 19 shows differences in the ordering of both the occupied and unoccupied magnetic orbitals and in the composition of the higher S orbitals as well as in $16a_1$. (Reference 19 corresponds to SH toward $\hat{z}$, with $\theta = 24.5°$.) These differences are largely a consequence of the different assumed geometry, rather than computational differences.

We believe that such variations with SR group orientation constitute an important physical feature of ferredoxin electronic structure. Different ferredoxin proteins can thereby be fine tuned for their specific catalytic or electron-transfer function. Unfortunately, at present there is insufficient structural and mechanistic evidence available to test this hypothesis adequately or to take more concrete observations. The only X-ray structure available for a 2-Fe ferredoxin protein is for an algal ferredoxin.[8] It has a structure with S-cysteine orientation intermediate to the theoretical geometries discussed above, but evidently the molecular and site symmetry is lower than C_{2v}. The g tensors of algal

(55) (a) Westheimer, F. H.; Kirkwood, J. G. *J. Chem. Phys.* **1938**, *6*, 513. (b) Cannon, R. D. *Chem. Phys. Lett.* **1977**, *49*, 299.

(56) Compare the theoretical results (labeled LSD–Xα) with experiment in: Wilk, L.; Vosko, S. H. *Phys. Rev. A* **1977**, *15*, 1839.

(57) McGarvey, B. R. In "Transition Metal Chemistry"; Carlin, R. L., ed. Marcel Dekker: New York, 1966; Vol. 3, pp 90–201.

Table VI. d → d Transitions for Reduced Ferredoxin Model, $Fe_2S_2(SH)_4^{3-}$

transition	type	ΔE_B	ΔE ($S = 1/2$)	experiment	J value (theory)
$16a_1^{\uparrow} \rightarrow 5a_2^{\uparrow}$	$d_{z^2} \rightarrow d_{xy}$	3310	2766	450-2000[a]	−209
$16a_1^{\uparrow} \rightarrow 11b_2^{\uparrow}$	$d_{z^2} \rightarrow d_{yz}$	4050	3346	3800, 4500[b]	−249
$16a_1^{\uparrow} \rightarrow 17a_1^{\uparrow}$	$d_{z^2} \rightarrow d_{x^2-y^2}$	4990	4467		−204
$16a_1^{\uparrow} \rightarrow 9b_1^{\uparrow}$	$d_{z^2} \rightarrow d_{xz}$	7590		5800, 6000[b]	

[a] From temperature dependence of Mossbauer QS for various proteins: Dunham et al., Munck et al., ref 5; Bertrand and Gayda, ref 14. [b] From optical spectroscopy for reduced spinach ferredoxin, adrenodoxin, respectively: Eaton et al., ref 7.

Table VII. Charge-Transfer Transitions for Oxidized Ferredoxin Model, $Fe_2S_2(SH)_4^{2-}$, Compared with Experimental Spectra

			experiment[a]	
transition	type	ΔE_B	optical	resonance Raman
$8b_1^{\downarrow} \rightarrow 16a_1^{\uparrow}$	S → Fe, spin forbidden	7300		
$10b_2^{\downarrow} \rightarrow 16a_1^{\uparrow}$	S → Fe, spin forbidden	9760		
$8b_1^{\uparrow} \rightarrow 16a_1^{\uparrow}$	opp. S, S* → Fe	10690	10700 (170)[b]	
$4a_2^{\uparrow} \rightarrow 16a_1^{\uparrow}$	S, S* → Fe, dipole forbidden	13380	12200 (260)[c]	
$10b_2^{\uparrow} \rightarrow 16a_1^{\uparrow}$	opp. S, S* → Fe	13870	13900 (800)[c]	
$8b_1^{\uparrow} \rightarrow 5a_2^{\uparrow}$	opp. S, S* → Fe	13980		
$8b_1^{\uparrow} \rightarrow 17a_1^{\uparrow}$	opp. S, S* → Fe	16350		
$4a_2^{\uparrow} \rightarrow 5a_2^{\uparrow}$	S, S* → Fe	16990	16900 (4800)[d]	
$10b_2^{\uparrow} \rightarrow 5a_2^{\uparrow}$	opp. S, S* → Fe	17260		
$4a_2^{\uparrow} \rightarrow 11b_2^{\uparrow}$	S, S* → Fe	18300		
$8b_1^{\uparrow} \rightarrow 9b_1^{\uparrow}$	opp. S, S* → Fe	18660		20490[e]
$10b_2^{\uparrow} \rightarrow 11b_2^{\uparrow}$	opp. S, S* → Fe	19270		
$10b_2^{\uparrow} \rightarrow 17a_1^{\uparrow}$	opp. S, S* → Fe	19910		
$4a_2^{\uparrow} \rightarrow 9b_1^{\uparrow}$	S, S* → Fe	21550		
$7b_1^{\uparrow} \rightarrow 16a_1^{\uparrow}$	S → Fe	21610		
$15a_1^{\uparrow} \rightarrow 11b_2^{\uparrow}$	opp. S → Fe	21790	22000 (9200)[d]	21000[e]
$10b_2^{\uparrow} \rightarrow 9b_1^{\uparrow}$	opp. S, S* → Fe	21890		
$15a_1^{\uparrow} \rightarrow 17a_1^{\uparrow}$	opp. S → Fe	22680		
$15a_1^{\uparrow} \rightarrow 9b_1^{\uparrow}$	opp. S → Fe	24150	24150 (11000)[d]	24210[e]
$3a_2^{\uparrow} \rightarrow 5a_2^{\uparrow}$	opp. S → Fe	24290		
$7b_1^{\uparrow} \rightarrow 5a_2^{\uparrow}$	S → Fe	25420		
$3a_2^{\uparrow} \rightarrow 11b_2^{\uparrow}$	opp. S → Fe	26120		
$3a_2^{\uparrow} \rightarrow 9b_1^{\uparrow}$	opp. S → Fe	29050		
$7b_2^{\downarrow} \rightarrow 16a_1^{\uparrow}$	Fe d → d, spin forbidden	30900		
$4b_1^{\downarrow} \rightarrow 16a_1^{\uparrow}$	Fe d → d, spin forbidden	35570		
$7b_2^{\uparrow} \rightarrow 16a_1^{\uparrow}$	Fe d → Fe d, charge transfer	38720		

[a] All energies are in cm^{-1}, molar extinction coefficients ϵ_m parentheses in units L mol^{-1} cm^{-1}. [b] From Eaton et al., ref 7, spinach ferredoxin. [c] From Rawlings et al., ref 59, spinach ferredoxin. [d] From Mayerle et al., ref 12a, synthetic analogue $[FeS(SCH_2)_2C_6H_4]_2^{2-}$. [e] From Adar, Blum, et al., ref 44, spinach ferredoxin and adrenodoxin.

ferredoxin have values close to those in spinach. For the synthetic models, highly accurate X-ray structures have been obtained for the oxidized, but not for the reduced, form. In principle, we would want to compare the physical properties and functions of ferredoxins (or synthetic analogues) having a known geometry and oxidation state. According to the argument above, the *S*-cysteine orientation alters the shape of $16a_1$ and consequently the *g* and *A* tensors. Moreover, the *S*-cysteine bond position in conjunction with the Fe–S bond will determine the location of the terminal S lone pairs (see Figure 3 for $10b_2^{\uparrow}$ and Figure 4), and by both electronic and steric interactions, it can influence the preferred direction of attack of an electron donor or acceptor.

d → d and Charge-Transfer Spectra. In Table VI, we compare our calculated spin-allowed d → d spectra with experiment for the ferrous site of reduced ferredoxin.[5,7,14] The experimental values 450–2000 cm^{-1} are determined indirectly from the temperature-dependent Mössbauer QS of various 2-Fe ferredoxins. The experimental higher energy transitions are those observed by optical spectroscopy for reduced spinach ferredoxin and adrenodoxin, respectively. We calculated the d → d spectrum by the Slater transition-state method, exciting from the lowest energy AF configuration of the reduced model to obtain energies ΔE_B (see also Figure 1). With additional Slater transition-state energies, exciting from the lowest energy F configuration (reduced) to higher d orbitals (Figure 5), we can also determine spin-projected $S = 1/2$ excitation energies $\Delta E(S = 1/2)$. Here we have used eq 5, 6, and 7 for each electronically excited state, and we have assumed that $c = 0.50$ for each state. Spin projection results in a small decrease in the predicted d → d energies. Generally, the agreement with experiment is quite good; the $d_{z^2} \rightarrow d_{xy}$ energy is higher than the experimental values by about 1500 cm^{-1}. The same method yields the *J* value of the Heisenberg spin ladder for each d → d excited state; the calculated *J* magnitudes are larger than in the reduced ground state. We know of no direct tests of this prediction.

We have also attempted to get an estimate of the intervalence charge-transfer transition energy (IVCT) for the reduced model; the assumed reduced-site Fe–S bond lengths were 0.07 Å longer than those of the oxidized site (see Experimental Section). The calculated IVCT energy was <0.05 eV (Slater transition state) in this geometry; the adiabatic electron-transfer energy as computed by Ziegler's method (the energy difference between AF states in the symmetric D_{2h} geometry and the asymmetric C_{2v} geometry above) was also <0.05 eV. There is then practically no vertical or adiabatic barrier to electron transfer from the calculations. Perhaps some barrier would exist if a full geometry optimization (or a more accurate calculation) were done, or by including other environmental effects such a hydrogen bonding. In any event, we predict a very low energy for the IVCT transition. Eaton et al.[7] have tentatively assigned a band at 11000 cm^{-1} in reduced proteins to the IVCT transition, but it appears that this is a S → Fe charge-transfer band as in oxidized ferredoxin. Cox[58] has considered the dependence of IVCT transition intensities on the initial total spin state *S* and on temperature for a Boltzmann distribution of spin states. Although we differ with some aspects of his analysis, we agree with his conclusions (expressed in eq 7 and 8 and Figure 3 of his paper). At low and moderate temperatures ($T \simeq 300$ K) the IVCT intensity in AF Fe^{3+}–Fe^{2+} systems with a $|J|$ of about 200 cm^{-1} is very low and increases slowly with temperature; $I(T)/I(\infty) \simeq 0.1$ when $kT/|J| = 1$. In

(58) Cox, P. A. *Chem. Phys. Lett.* **1980**, *69*, 340.

summary, the IVCT transition in 2-Fe ferredoxins is predicted to be weak and at very low energy, of order 0.1 eV.

We consider next the ligand-to-metal charge-transfer spectrum for the oxidized ferredoxin model as compared with the experimental spectrum, Table VII.[7,12,44,59,60] A number of workers have measured the experimental spectra of various ferredoxins and synthetic analogues. Qualitatively, the spectra are similar, but there are quantitative differences. Because of the diverse systems and spectral regions studied, we have collected some of the best defined data from ferredoxins and synthetic analogues in Table VII. Considerable disagreement exists on spectral assignments below 14 000 cm^{-1} where a set of weak peaks and shoulders is found;[7,59,60] the absorption intensity rises rapidly above 16 500 cm^{-1}, clearly due to a large number of dipole-allowed sulfur → Fe charge-transfer bands.[12,60]

All calculated energies were determined by the Slater transition-state method starting from the initial AF configuration (oxidized). (Notice that there will be an equivalent set of transitions to the ones given in Table VII, where the spin index of both the initial and the final orbital of transition are reversed. These transitions are mirror images.) We have mainly considered the spin- and dipole-allowed spectrum; in addition, the two lowest energy spin-forbidden transitions $8b_1^{\downarrow} \rightarrow 16a_1^{\uparrow}$, and $10b_2^{\downarrow} \rightarrow 16a_1^{\uparrow}$ and the lowest dipole forbidden transition $4a_2^{\uparrow} \rightarrow 16a_1^{\uparrow}$ were calculated. The spin-forbidden transitions are predicted as the lowest energy transitions overall, and are primarily near neighbor S → Fe charge transfer. (We have designated the (terminal) near-neighbor, bridge, and farthest sulfur from a given Fe by S, S*, opp. S, respectively.) The lowest energy dipole-allowed transition $8b_1^{\uparrow} \rightarrow 16a_1^{\uparrow}$ is assigned to the weak band observed at 10 700 cm^{-1} in spinach ferredoxin. This band assignment deserves comment. Eaton et al.[7] have measured a fairly large anisotropy factor from circular dichroism for this band, consistent with a spin-allowed and magnetic dipole-allowed transition. The transitions $8b_1^{\uparrow} \rightarrow 16a_1^{\uparrow} \rightarrow 4a_2^{\uparrow} \rightarrow 16a_1^{\uparrow}$ and $10b_2^{\uparrow} \rightarrow 16a_1^{\uparrow}$ which we predict in this vicinity are both spin and magnetic dipole allowed. In an earlier paper, Palmer et al.[60] noticed significant circular dichroism in the 13 900-cm^{-1} (ϵ = 800) band, which we have assigned to $10b_2^{\uparrow} \rightarrow 16a_1^{\uparrow}$ (optically active) plus $8b_1^{\uparrow} \rightarrow 5a_2^{\uparrow}$ (optically inactive). Rawlings et al.[59] have assigned the 13 900-cm^{-1} band as a spin-forbidden d → d band on energetic grounds, but this is contradicted by the observed optical activity.

The lowest energy dipole-allowed transitions are of the type opp. S, S* → Fe and terminate in the $16a_1$ or $5a_2$ orbital (e representation in an idealized T_d site symmetry). Dipole transitions involving near-neighbor S → Fe occur at higher energy (for example, $4a_2^{\uparrow} \rightarrow 5a_2^{\uparrow}$ and $7b_1^{\uparrow} \rightarrow 16a_1^{\uparrow}$) as do transitions terminating in the higher d orbitals of the t_2 set ($11b_2$, $17a_1$, and $9b_1$). In addition to the optical spectrum, resonance Raman spectra[44] of oxidized ferredoxin proteins have been measured with exciting radiation of 20 490, 21 000, and 24 210 cm^{-1}. We have assigned these mainly to transitions terminating in the t_2 set, and originating from opposite S or S*; the relevant theoretical energies are in good agreement with experiment. In the resonance Raman process, both vibrational transitions and transitions between spin states of the Heisenberg spin ladder can occur upon re-radiation back to the ground electronic state manifold.[44,61] The corresponding vibronic matrix elements are larger if the upper electronic state is antibonding (t_2) rather than nonbonding (e) in accordance with the assignments above.[61] More surprising is the prediction based on the resonance Raman intensities for the spin transitions that the resonance Raman band at 20 490 cm^{-1} (488 mm) has greater bridging sulfur (S*) involvement than the other two bands.[44] This is based simply on the greater involvement of S* in the superexchange mechanism of magnetic coupling. This suggestion is in very fine agreement with our resonance Raman band assignments. Notice that $4a_2^{\uparrow}$, $8b_1^{\uparrow}$, and $10b_2^{\uparrow}$ all have considerable S* density (32% to 48%) while $15a_1^{\uparrow}$ has little S* density (10%).

The presence of the low-lying spin-forbidden S → Fe charge-transfer transitions ($8b_1^{\downarrow} \rightarrow 16a_1^{\uparrow}$ and $10b_2^{\downarrow} \rightarrow 16a_1^{\uparrow}$) in our 2(Fe–S) calculations closely parallels the lowest energy excitations expected from Norman and Jackel's[16] Xα–SW study of 1(Fe–S) models (see their energy level diagram for spin polarized $Fe(S\text{-}CH_3)_4^-$ and discussion). Similarly, in Bair and Goddard's[15] HF–CI study of $Fe(SH)_4^-$, the lowest energy excitations are spin forbidden with predicted energies from 7900 to 12 700 cm^{-1}. Although in the latter study these transitions are assigned as Fe d → d spin forbidden, the presence of Fe–S covalency in both the singly and doubly occupied orbitals (as found by Bair and Goddard) implies a closer correspondence with the Xα results for 1-Fe and 2-Fe models than is apparent from the assignments. (Moreover, the detailed chemical analysis of such large-scale CI calculations is difficult.) We find that the actual spin-forbidden Fe d → d transitions occur at much higher energy; for example, $7b_2^{\downarrow} \rightarrow 16a_1^{\uparrow}$ has an energy of 30 900 cm^{-1}.

A comparison of the experimental dipole and spin-allowed sulfur → Fe charge-transfer excitations shows that these begin at lower energy in oxidized ferredoxin than in rubedoxin. The relevant energies are 10 700–13 900 cm^{-1} in ferredoxin[7,59] and 15 000–18 000 cm^{-1} in rubedoxin.[15,62] The low-energy transitions $8b_1^{\uparrow} \rightarrow 16a_1^{\uparrow}$, $10b_2^{\uparrow} \rightarrow 16a_1^{\uparrow}$, and $8b_1^{\uparrow} \rightarrow 5a_2^{\uparrow}$ are specific to the dimer.

Relationship between Optical Spectra and Electron Transfer. Finally, we will briefly assess the possible relationship between the mechanism of electron transfer in ferredoxins and the presence of low-lying sulfur → Fe charge-transfer transitions. Because different ferredoxins can function as electron transport agents in the respiratory chain, in photosynthesis, or in catalytic electron transfer, it is unlikely that any single mechanism applies to all.[2,3] We can distinguish between situations where the immediate source of electrons for oxidized ferredoxin is hydrogen, most likely in the respiratory chain, and others where the added electron comes from a negatively charged donor molecule, likely in photosynthesis.[2]

We consider first the response of an oxidized ferredoxin dimer active site to a negatively charged donor. In algal ferredoxin, the X-ray structure shows that both Fe centers are surrounded by hydrophobic residues as well as being coordinated to cysteine and bridging sulfurs.[8,41] Since there is no direct access to Fe by the solvent, it is unlikely that a charged donor could get close enough to directly transfer an electron into the Fe $3d_{z^2}$ orbital ($16a_1$). By contrast, two cysteine sulfurs neighboring a single Fe are exposed to the solvent,[8,41] making an indirect electron-transfer process possible. The electric field of the charged donor will cause a polarization of oxidized ferredoxin, effectively creating an internal cysteine S → Fe ($3d_{z^2}$) charge transfer. The resulting sulfur hole can then be filled by direct electron transfer from the donor. The polarizability is simply

$$P_i = 2e \sum_{s \neq n} \frac{|M_{isn}|^2}{E_n - E_s}$$

where i = $\hat{x}$, $\hat{y}$, and $\hat{z}$, and E_s and E_n are the excited and ground-state energies, respectively, and M_{isn} is the electric dipole transition moment—the same terms that enter into the charge-transfer spectrum. The analogy is only qualitative since the donor electric field is not constant, but clearly the presence of low lying (dipole-allowed) charge-transfer states is important. Moreover, the direction of approach of the donor to the cysteine sulfur plays a role analogous to the electric field polarization direction in the optical spectrum. One curiosity is that the lowest lying dipole transitions proceed across the molecule, opp. S, S* → Fe, so that the distant Fe site is reduced. It would be interesting to see if this has any important physical consequences. Judging from the charge-transfer spectrum, there should be a significant energy barrier for indirect electron transfer (compared with direct reduction of Fe). The electron-transfer probability is then enhanced

(59) Rawlings, J.; Siiman, O.; Gray, H. B. *Proc. Natl. Acad. Sci. U.S.A.* **1974**, *71*, 125.
(60) Palmer, G.; Brintzinger, H.; Estabrook, R. W. *Biochemistry* **1967**, *7*, 1658.
(61) Theory of resonance Raman: (a) Heller, E. J. *Acc. Chem. Res.* **1981**, *14*, 368. (b) Lee, S. Y.; Heller, E. J. *J. Chem. Phys.* **1979**, *71*, 4777.
(62) Eaton, W. A.; Lovenberg, W. In ref 1, Vol. 2, pp 131–162.

by a high-energy donor; these are characteristic of photosynthetic systems.

Where atomic hydrogen is the electron source, there is no necessary barrier for indirect electron transfer. Our proposed initial step is S–H bond formation with cysteine sulfur (notice the sulfur lone pairs and partial radical character); this can be characterized as reductive addition of H to $Fe_2S_2(SR)_4^{2-}$. The fully reduced form is attained after deprotonation: $H + F_2S_2(SR)_4^{2-} \rightarrow HFe_2S_2(SR)_4^{2-} \rightarrow H^+ + Fe_2S_2(SR)_4^{3-}$. According to Mitchell's chemiosmotic theory,[2,63] ATP synthesis by the respiratory chain requires a combination of a $[H^+]$ gradient and an electrostatic potential gradient across the mitochondrial membrane; the species $HFe_2S_2(SR)_4^{2-}$ can contribute to the electrostatic potential and requires less energy to form than the fully reduced form. Spectroscopically, $HFe_2S_2(SR)_4^{2-}$ should be distinguishable from either $Fe_2S_2(SR)_4^{2-}$ or $Fe_2S_2(SR)_4^{3-}$, so that studies of whether the H-bonded form is prevalent in functioning membranes (under steady-state conditions) would be valuable, as would studies of the corresponding synthetic analogues. We expect to do calculations on the model complex $HFe_2S_2(SH)_4^{2-}$ in the near future.

Returning to the deprotonation step, the intriguing possibility is that the deprotonated H is not the same as the H atom added originally. Instead, it could come from one of the many hydrogen bonds between the protein residues and cysteine sulfurs. Therefore, hydrogen could arrive at one end of the complex (at one set of 2(SR)) and protons could leave from the opposite end (the other 2(SR) groups). Effectively a neutral [H] gradient is converted into a $[H^+]$ gradient by ferredoxin, leaving the latter in the 3^- form.

The electron-transfer mechanisms suggested above should be specific enough for experimental tests.

Acknowledgment. We thank J. G. Norman, J. Osborne, D. Case, and A. Aizman for communicating results prior to publication, E. R. Davidson and A. Trautwein for discussions, A. Liechtenstein for correspondence, and Pieter Vernooijs for computational assistance. This investigation was supported by The Netherlands Foundation for Chemical Research (SON) with financial aid from The Netherlands Organization for the Advancement of Pure Research (ZWO). At the University of Washington, Louis Noodleman is grateful to the donors of the Petroleum Research Fund, administered by the American Chemical Society, for financial support from a grant to J. G. Norman.

Appendix

In this appendix we consider the dependence of the interaction matrix element $\langle\psi_L(S)|H|\psi_R(S)\rangle$ on S. We obtain $\psi_{L,R}(S)$ by spin projection from $\psi_{L,R}(B)$ given in eq (3), and normalizing

$$\psi_R(S) = \frac{1}{\sqrt{N(S)}} {}^S_M O \psi_R(B) \qquad \text{(A-1)}$$

where ${}^S_M O$ is the spin projection operator and $1/N^{1/2}$ the normalization constant. When we expand $\psi_R(B)$ we get a leading determinant $\phi_0{}^R$ (eq 3), and terms in c, c^2 etc.:

$$\langle\psi_L(S)|H|\psi_R(S)\rangle = N^{-1}\langle {}^S_M O\phi_0{}^L + \sum_i c_i {}^S_M O\phi_i{}^L + \ldots |H| {}^S_M O\phi_0{}^R + \sum_j c_j {}^S_M O\phi_j{}^R + \ldots) \qquad \text{(A-2)}$$

If c_i is small, the leading term is

$$N^{-1}\langle {}^S_M O\phi_0{}^L|H| {}^S_M O\psi_0{}^R\rangle = N^{-1}\langle\phi_0{}^L|H| {}^S_M O\phi_0{}^R\rangle \qquad \text{(A-3)}$$

The spin projection of $\phi_0{}^R$ leads to an expansion in determinants that differ from $\phi_0{}^R$ in permutation of α and β spin labels:

$$\frac{1}{\sqrt{N}} {}^S_M O\phi_0{}^R = \frac{1}{\sqrt{N}}(x_0\phi_0{}^R + \sum_p x_p\phi_p{}^R) \qquad \text{(A-4)}$$

where the coefficients x_0 and x_p depend on S. From normalization, and using the turn over rule on ${}^S_M O$ and its idempotency:

$$\left\langle \frac{1}{\sqrt{N}} {}^S_M O\phi_0{}^R \middle| \frac{1}{\sqrt{N}} {}^S_M O\phi_0{}^R \right\rangle = \frac{1}{N}\langle\phi_0{}^R|{}^S_M O\phi_0{}^R\rangle = N^{-1}\langle\phi_0{}^R|x_0\phi_0{}^R + \sum_p x_p\phi_p{}^R\rangle = x_0/N = 1 \qquad \text{(A-5)}$$

$$\psi_R(S,M) = \sqrt{N}\phi_0{}^R + \sum_p (x_p/\sqrt{N})\phi_p{}^R \qquad \text{(A-6)}$$

The important determinant in this expansion is the one that matches $\phi_0{}^L$

$$\phi_0{}^L = |(\text{rest})(d_1{}^L\alpha d_1{}^L\beta)d_2{}^L\beta \ldots d_5{}^L\beta;\ d_1{}^R\alpha \ldots d_5{}^R\alpha| \rightarrow \phi_{p_0}{}^R = |(\text{rest})d_1{}^L\alpha d_2{}^L\beta \ldots d_5{}^L\beta;\ (d_1{}^R\alpha d_1{}^R\beta)d_2{}^R\alpha \ldots d_5{}^R\alpha| \qquad \text{(A-7)}$$

The matrix element between $\phi_0{}^L$ and $\phi_{p_0}{}^R$ is essentially a hopping integral between $d_1{}^L$ and $d_1{}^R$. The S dependency of the interaction matrix element is in $N(S) = x_0(S)$ and $x_{p_0}(S)$:

$$\langle\psi_L(S)|H|\psi_R(S)\rangle \simeq (x_{p_0}(S)/N(S))\langle\phi_0{}^L|H|\phi_{p_0}{}^R\rangle \qquad \text{(A-8)}$$

N and x_{p_0} are easily obtained when we realize that eq A-6 is in fact a vector coupling equation:

$$|SM\rangle = \sum_{M_1,M_2} \delta(M_1 + M_2, M)\langle S_1M_1S_2M_2|SM\rangle|S_1M_1\rangle|S_2M_2\rangle \qquad \text{(A-9)}$$

where $\phi_0{}^R$ is $|{}^5/_2\ {}^5/_2)_L|2{-}2)_R$ (see eq 3) and $\phi_{p_0}{}^R$ is a determinant in the expansion of $|{}^5/_2 - {}^3/_2)_L|2{-}2)_R$. We obtain

$$x_{p_0}/N = \frac{x_{p_0}/\sqrt{N}}{\sqrt{N}} = \frac{\langle {}^5/_2 - {}^3/_2;\ 2 - 2|SM\rangle/\sqrt{5}}{\langle {}^5/_2\ {}^5/_2;\ 2 - 2|SM\rangle} = \frac{S + {}^1/_2}{5} \qquad \text{(A-10)}$$

from which we conclude that $\langle\psi_L(S)|H|\psi_R(S)\rangle$ and therefore the g, u splitting is proportional to $(S + 1/2)$.

(63) Mitchell, P. *Biol. Rev. Cambridge Philos. Soc.* **1966**, *41*, 445.

Registry No. $Fe_2S_2(SH)_4^{2-}$, 69509-17-7; $Fe_2S_2(SH)_4^{3-}$, 71966-82-0.